January 2014

Effects Of Stress Ratios On Polymer Composite Fatigue

Mohammad Rasheduzzaman

EFFECTS OF STRESS RATIOS ON POLYMER COMPOSITE FATIGUE

by

Mohammad Rasheduzzaman

Bachelor of Science, Bangladesh University of Engineering & Technology, Dhaka, 2008

A Thesis

Submitted to the Graduate Faculty

of the

University of North Dakota

in partial fulfillment of the requirements

for the degree of

Master of Science

Grand Forks, North Dakota
December
2014

This thesis, submitted by Mohammad Rasheduzzaman in partial fulfillment of the requirements for the Degree of Master of Science from the University of North Dakota, has been read by the Faculty Advisory Committee under whom the work has been done and is hereby approved.

_____
Chairperson (Dr. Matthew Cavalli)

_____
Dr. Surojit Gupta

_____
Dr. William Semke

This thesis meets the standards for appearance, conforms to the style and format requirements of the Graduate School of the University of North Dakota, and is hereby approved.

_____
Wayne Swisher
Dean of the Graduate School

_____
Date: 12-10-2014

PERMISSION

Title EFFECTS OF STRESS RATIOS ON POLYMER COMPOSITE FATIGUE

Department Mechanical Engineering

Degree Master of Science

In presenting this thesis in fulfillment of the requirements for a graduate degree from the University of North Dakota, I agree that the library of this University shall make it freely available for inspection. I further agree that permission for extensive copying for scholarly purposes may be granted by the professor who supervised my thesis work or, in his absence, by the chairperson of the department or the dean of the Graduate School. It is understood that any copying or publication or other use of this thesis or part thereof for financial gain shall not be allowed without my written permission. It is also understood that due recognition shall be given to me and to the University of North Dakota in any scholarly use which may be made of any material in my thesis.

Signature Mohammad Rasheduzzaman

Date 12-10-2014

Contents

LIST OF FIGURES

LIST OF TABLES

ABSTRACT

In this work, fatigue behavior of glass fiber composite has been being investigated at different stress ratios and compared them with some previous model from literature. Ten layers of unidirectional glass fibers are used. Glass fibers and resin were supplied by LM Wind Power, a leading manufacturer of wind turbine blades. The plates were made by the VARTM (Vacuum Assisted Resin Transfer Molding) process to control fiber volume fraction and void content. Specimens were then post cured. Volume fraction was determined by burn off test and material strength by 4 point bending static testing. Four point bending fatigue tests were conducted at different stress ratios (min stress/max stress). S-N curve analysis, stiffness degradation analysis, model fit with desirable fatigue model and image processing has performed. This research is showing a transition of failure mechanism with the variation of maximum applied stress.

CHAPTER ONE: INTRODUCTION

There are four basic categories in structural materials: metals, polymer, ceramics and composites [1]. Composites can be made by various combinations of the three other material classes, which results in different properties. The earliest composite materials used by humans, were in macroscopic range. As the technology has improved the size of the phases in composite materials are decreasing. Today, nano-composite materials play a vital role in research and industry. Carbon nanoparticles, nano-fibers, nanotubes are well-renowned materials for their unique properties.

Fiberglass is one of the first modern composite materials which is used in boat hulls, sports equipment, etc. Fiberglass reinforcement is very effective as many materials are stronger and stiffer in fiber form than in bulk form. Griffith [1] showed that as the rods and fibers got thinner they got stronger. The reason of this phenomenon is thinner rods and fibers are less diameter which causes less probability of failure that arises from surface cracks. Composite materials typically comprise two basic components, one is matrix and other is reinforcements.

Metallic Oxides and silica are two raw materials for making glass fibers [1]. Mixture of these two are heated drawn by mechanically through a small orifice. E-glass is popular for its electrical properties and is commonly used in industry. For matrix materials polymers, metals and ceramics can be used. The matrix protects fibers from structural damage, hold them and distributes the applied or external load to the fibers. Ductility, toughness, and electrical insulation are common necessary properties for matrix materials depending upon their uses. To avoid unexpected reactions between matrix materials and fibers, they should be chemically compatible.

Examples of composite uses include automotive, aerospace, marine, architectural structure, and consumer products as skis, golf clubs, and tennis rackets [1]. They are widely used in aerospace industry because their specific strength and stiffness are higher than conventional metals.

When a material is selected for design for a particular application, the properties of this material must be known. Various test methods are available to measure the properties according to their application and material. Static tests give an idea about the materials strength but almost all practical applications have some degree of variable load conditions. To design properly, it is needed to know the properties, strength or fracture behavior of a material in relevant loading conditions.

Structural materials commonly fail by fatigue [2]. Fatigue is a phenomenon in which failure is observed at cyclic stress below the yield point. To induce fracture, some portion of local cyclic stresses must be tensile [2]. Applications like aircraft parts, rotating axle of automobiles, and turbine blades are all prone to fatigue. Some applications may not seem to experience cyclic loading but actually they do. An example is a bridge after a long service period. The varying load in the bridge may be the self-weight or different traffic density. Dealing with fatigue in engineering designs still is a challenging job and the only option to overcome this challenge is test the design material under cyclic loading.

CHAPTER TWO: BACKGROUND

To determine a material's service life, one must first define when the life will end or the part will fail. This requires the choice of failure criterion. For composite materials, this is more complicated than for conventional metals. Failure in composites can depend on fiber direction, volume fraction, materials type, etc. For example, unidirectional and woven composites give different failure stress values for the same loading condition. Also, different number of ply gives different strength. Tsai-Hill, Tsai-Wu [1] are the common failure criteria for composite materials. From the properties of matrix and fiber, ply stress can be determined for a particular loading condition. These ply stresses need to be compared with a failure criteria. Minimum safety factor among the ply stress give the maximum allowable stress for the material.

2.1 Previous works on composite fatigue

One of the main reasons to study the fatigue behavior of materials to find a model that can be applied in engineering applications. However, fatigue damage mechanism and failure prediction is not simple.

Various researches has been done in the field of fatigue testing of different materials, including composite materials. Examples include fatigue life assessment [3, 4], damage modeling and propagation of failure [5, 7, 8, 11-15], effect of stress in off-axis fibers [6], Failure Criteria [5, 9], developing models for fatigue life prediction [16, 19-21].

2.1.1. Computational Work

Eric Hanus and Torsten Ericsson have discussed computational modeling of fatigue in composite [10]. According to the authors, in the engineering design field, the safety factor is used for composite materials are almost same as metal. But composite materials are not as homogeneous as metals due to reasons like fiber misalignment, void, porosity, technician's faults, etc. So it is necessary for design with composite materials to know the life cycle in fatigue [10]. Makeev and Nikishkov [3] presented an approach to know the fatigue life of composites without destroying them. They use CT (Computed Tomography) which is a non-destructive evaluation technology to determine the manufacturing defects including wrinkles and voids. There are some several assumptions that were used to calculate the dimensions of different defects [3]. A finite element model was developed after the detection of defects. As composite materials are highly anisotropic, a three dimensional stress-strain relationship was required for this modeling.

Makeev et al [29] shows a method called simple short-beam shear (SBS) test which is capable to determine 3D consecutive properties with the help of Digital Image Controller. To inform the aerospace industry about this new method that identify defects and find life time based upon this study, is one of the main objectives of authors [3]. The main success of this work is the very few samples needed for SBS test which can characterize the materials. Among various critical issues in aerospace industry, to design and built a part at the first time that would be sustaining fatigue. First time yield for designs is around 20%-30% and 70%-80% in production [3]. That means around 20%-30% designs have passed at first time after design and 70%-80% have passed in the production phase. This is really difficult for designers as there is no particular tool or method for this. This method developed by the authors will successfully predict the fatigue life.

Lifetime in fatigue also can be determined by progressive damage modeling (PDM). Labeas and others discussed a method based on a similar procedure [5]. In conventional PDM, a large amount of post-processing is required this is impractical for large-scale structures. The study of Lubeas et al. a small-scale damage topology was compared with large structure and appropriate modifications of this data were used with classical PDM methodology. In the large-scale structure, numerical modeling required a large amount of computational effort. After the initial numerical results are achieved, post-processing takes significant time due to a large number of DOF's. For this reason, there is no published works that demonstrate this large computation in a large structure. Lubeas et al. presented a method to overcome this problem with large structure [5]. Proper modifications have been made in the classical PDM methodology in order to apply damage initiation and progression in the large composite structure. Stress analysis is performed by a sub modeling technique. The proposed modification in the PDM applies generic shear joints. One key conclusion is that to determine large scale structural behavior damage evolution is crucial and it is impractical to identify damage evolution without the proposed method [5].

2.1.2 Influence of Mean Stress

Kawai and Suda [6, 19] demonstrated the influence of mean stress on unidirectional composites. To perform experiments, they used carbon epoxy coupons.

$$\text{Mean stress} = (\text{Max Stress} + \text{Min Stress})/2 \qquad \text{Eqn (2.1)}$$

A model to determine the number of cycles was proposed:

$$n(R) = A \exp\left(\frac{1}{1-R}\right) \qquad \text{Eqn (2.2)}$$

Where A is a material constant and the absolute value of R should be less than 1.

The results of the study support the idea that the relative fatigue strength of a particular type material becomes lower with the decreasing stress ratio [6].

2.1.3 Cumulative Damage Model

Subramanian et al. [11] proposed a cumulative damage model to predict fatigue life. They conducted experiments on a composite laminate with a $(0,90_3)$ layup. They found that most of the stiffness degraded after 10% of the life of a sample. Below 10%, most of the crack growth occurs in the 90 degree ply. After that, fatigue life depends mostly on the 0 degree ply. A pre-defined S-N curve for the 0 degree ply provided data for further investigations. The authors proposed Eqn (1.3) to be used to calculate the changes in interfacial efficiency with cycles. The term interfacial efficiency is used to model the degradation of the interface under fatigue loading [11]. The change in the efficiency is a function of cycles that estimated from Stiffness reduction data.

$$\dot{\eta}= 0.76- e^{7 \log(n)} \qquad \text{Eqn (2.3)}$$

A damage parameter can be calculate by the following equation

$$D(n)= 1-(E(n)/E_o) \qquad \text{Eqn (2.4)}$$

Where, n is the no of cycles, E(n) is stiffness after n cycles, and E_o initial stiffness.

2.1.4 CG Method

A new methodology for predicting fatigue of fiber reinforced plastic (FRP) laminates based on the evolution of the center of gravity (CG) of the hysteresis loop has been proposed [4,17]. This method can be applied by testing only one sample. The CG method is an alternative approach to S-N curve to finding the fatigue life [4].

Hysteresis loop evolution is an important indicator of the degradation of a material's properties during fatigue testing. Displacement, stiffness and dissipated energy can be summarized from HL. If the evolution of the HL can be studied during fatigue testing then any sudden change in the evolution can be determined. This can be linked to the failure of the coupons.

The HL evolution curve has been identified as a new parameter to determine the degradation properties. Momenkhani and Sarkani [4, 17] introduced a new method, the CG method that is very useful to determine damage accumulation. For every HL, there is point that has influence at every point upon this graph and this is called CG of this particular HL. Equation [] can be used to find the CG of each HL curve.

$$X_{CG} = \frac{1}{A} \iint X \, dA \, Y_{CG} = \frac{1}{A} \iint Y \, dA \qquad \text{Eqn (2.5)}$$

where, A is area under the HL curve.

After getting all the CG of every HL and connecting them there is a trend line will be observed. Several straight lines can be drawn by connecting the CGs; each line represents a particular stress ratio. Fatigue damage of FRPs can be determined by studying these straight lines. Each curve can be created by testing only one specimen.

The CG method is not dependent on the number of cycles. To correlate the no of cycles between CG, it is necessary to plot a graph. The graph would be X component of the CG at the failure points at different stress level Vs the no of cycles at failure. Figure [2.1] represents the graph.

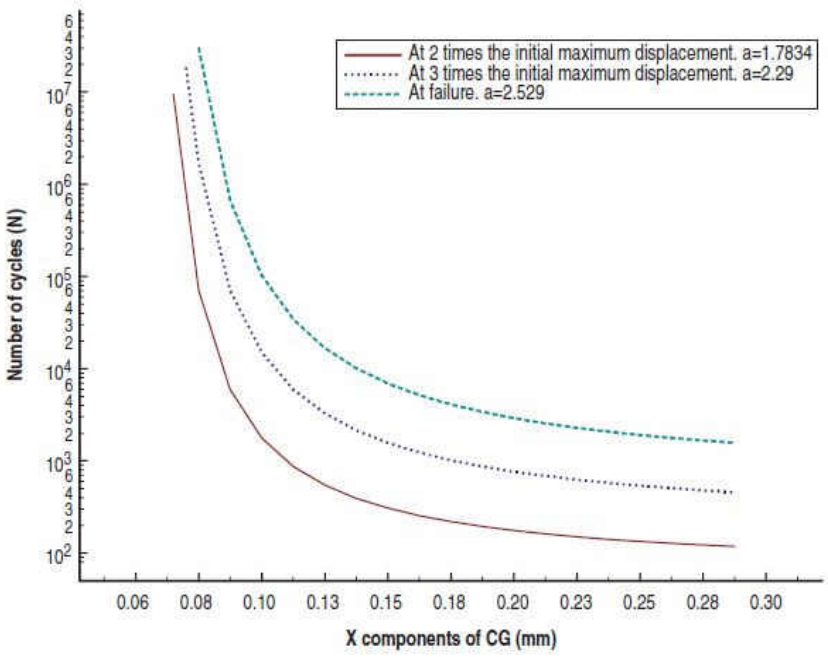

Figure 2.1 : X component of CG vs Number of cycles [4]

Fatigue life of untested stress ratio can be predicted by the relationship among the x component of CG at specific points vs. the no of cycles according to:

$$\text{Log}(N) = a\, e^{0.0762/X_{CG}} \qquad \text{Eqn(2.6)}$$

where, a represents a model parameter that can be obtained from experimental data.

By testing only one sample at each stress level all information can be calculated. The DL is first identified for a low stress level. After DL line is created, the test can be stopped and can be performed at another stress level. Repeating this procedure to low to high stress ratios allows the CG method to be applied.

2.1.5 Power Law Model

In the field of fatigue of analysis, the power law model [30] is extensively used for the metals. This model can also be used for composite materials in some cases. The power law model is shown in Eqn (2.7).

$$N S^m = K \qquad \text{Eqn (2.7)}$$

Here, S and N represent stress and cycle respectively. K and m are material properties. They can be determined from experimental data by linear regression of log(S) and log (N). Figure [2.2] shows a typical S-N curve.

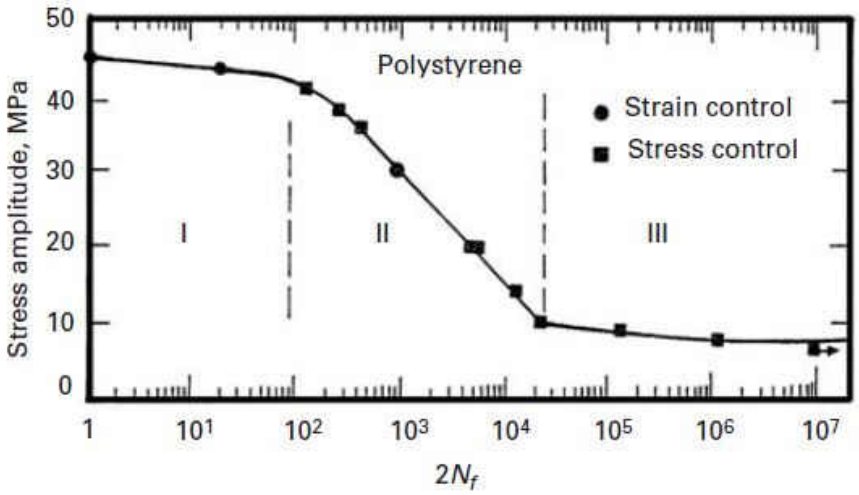

Figure [2.2]: Typical S-N curve [2]

A modified power law relationship has been used for FRP; it is called the Manson-Coffin relation and is shown in Eqn (2.8).

$$sN^d = c \qquad \text{Eqn (2.8)}$$

where, d and c are model parameters and s is ratio of applied stress and the ultimate strength:

$$s = S / S_{ult}$$

2.1.6 Inverse Power Law Model

Hwang and Han [4] proposed another relationship of S-N curve model which the referred to as the inverse Power low model.

$$N = [B\ (1-S)]^{1/c} \qquad \text{Eqn (2.9)}$$

Where, B and c are fitting parameters. Observations made from the data of Hwang and Han [26] fitted best with the model in the low cycle (10^5) fatigue region. Howson et al. [27] shows the data range that fit is more than 10^5 and less than 10^6.

2.1.7 Stiffness Degradation

When a material undergoes fatigue loading there is some cracking and fracture initiated at the microscopic scale. This can be happen for a number of reasons including matrix cracking, fiber de-bonding, fiber fracture and ply delamination. As a result, some reduction occurs in the stiffness of this material. Yang et al [28] shows an approach called the residual stiffness approach. The assumption of this approach is that degradation of the stiffness can be expressed as a power function of the number of cycles. The expression is shown in Eqn (2.10).

$$\frac{dE_n}{dn} = -E_0 Q v n^{v-1} \qquad \text{Eqn (2.10)}$$

Where, E_0 and $E_n$represent the initial stiffness and stiffness after n cycles, respectively. Q and v are model parameters that depend on loading frequency, stress ratio, applied stress and the environment.

2.1.8 Fatigue Damage model

Fuqiang and Weixing [12] presented a fatigue damage model of composites based on the stiffness degradation method using two parameters. The relationship between the parameters and the fatigue life of the composite is proportional and inversely proportional, respectively, with the fatigue loading level. Fatigue loading level is the combination of maximum stress and ratio. The authors propose that the residual fatigue life can be determined from 4 sets of two level

experimental data. Under cyclic loading, structural changes develop at the micro-scale in composite and cannot be reversed. When the number of cycles increases continuously structural changes also increases and initiate a failure. As the micro-scale change increase, the strength and material stiffness also change. The authors assumed that when the initial load is applied to the composite a crack first developed in the matrix region and, with increasing load cycles, this matrix crack grows into fiber region. As a result, the material suddenly fails. To determine the changes of Young's modulus, a stiffness degradation technique can be applied. Using this stiffness degradation model, one can find the fatigue life at the middle or at end of life of a composite material. The proposed model of the damage is showing in Eqn (2.11):

$$D(n) = (E_0 - E(n))/(E_0 - E_f) = 1-(1-(n/N)^B)^A \quad \text{Eqn (2.11)}$$

Where, E_0= initial Young's modulus, E_f= failure Young's modulus, N is the fatigue life, n is the life cycle at an instant time. A and B are model parameters and they are determined statistically from experimental data. D(n) is a damage development parameter.

At every cycle, this parameter depends on the previous load cycle. The authors proposed a cumulative damage accumulation parameter n_i.

$$D(n_i) = 1- \left(1 - \left(\frac{n_i+n_{i,i-1}}{N_i}\right)^{B_i}\right)^{A_i} \quad \text{Eqn (2.12)}$$

$$n_{i,i-1} = N_i\left(1 - \left(1 - \left(\frac{n_{i-1}+n_{i-1,i-2}}{N_{i-1}}\right)^{B_{i-1}}\right)^{\frac{A_{i-1}}{A_i}}\right)^{1/B_i} \quad \text{Eqn (2.13)}$$

A_i, A_{i-1}, B_i, B_{i-1} are the parameters under the ith and (i-1)th fatigue loading, respectively. $n_i$andn_{i-1} are the cycles under the ith and (i-1)th loading cycles. $N_i$andN_{i-1} are the fatigue lives corresponding to the ith (i-1)th applied loadings.

Another damage model was presented by Mao and Mahadevan [13]. They proposed:

$$D = q(\frac{n}{N})^{m}_{1} + (1-q)\,(\frac{n}{N})^{m}_{2} \qquad \text{Eqn (2.14)}$$

where, D is normalized accumulated damage and q, m_1, m_2 are material dependent parameter. n is the number of applied loading cycles and N is the fatigue life.

2.1.9 Strength Degradation Concept

Both the strength as well as elastic moduli decrease with fatigue damage. Halpin et al. [31] suggest a method to find of damage of composites by residual strength. Yang et al. [32, 33] and Yang and Jones [34] have done a lot of work on a residual strength approach. Eqn (1.15) is suggested by Yang and jones [34].

$$Ds_r/dn = -AS_r^{1-p}/P \qquad \text{Eqn (2.15)}$$

where A and P are model parameters. Researchers suggest that there is a dependency of A upon the applied stress at the nth cycle and initial ultimate strength.

2.1.10 Damage Mechanics Model

Wenjing et al. [14], present a model by which fatigue life of fiber reinforced polymer can be found. A continuum damage evolution equation has been developed analytically and coefficients of that equation were determined by the fatigue testing of 0° and 90° unidirectional laminates. Fatigue test data were generated for off-axis unidirectional laminates and was compared with model data. E-glass fiber and polyester resins GT200(GFRP) were used. 30° and 45° fiber orientations were used for the samples and the fatigue test was conducted under tensile stress with ratio R=0.1.

To derive this continuum model, the authors first assume is that damage of the composite lamina can be represented as damage of the fibers and of the matrix. They included two independent

variables; one is damage degree of fibers and other is damage degree of matrix. Then the overall stiffness matrix for the lamina was established with these two parameters and other properties of the fibers and matrix. The authors used a thermodynamic relation [14] where the damage driving force is claimed as a thermodynamic relationship. After some algebraic manipulation, a relation was developed for fibers and matrix separately. This equation is called the damage evolution equation and parameters of this equation can be determined by experiment.

The damage evolution equation's parameters for the matrix and fibers were determined by the fatigue experiments. It is assumed by the authors that in a 90° unidirectional laminate the fatigue life mainly depends on the matrix. The up and down method was used for the fatigue limits. Up and down method is a statistical technique. By this method if one sample sustain in a loading condition then that sample tested further by increasing the applied stress [35]. The same procedure was used for finding the parameters of the damage evolution equation for the fibers. 0° unidirectional laminate were used by assuming that fatigue life of that entirely depend on fiber life.

After finding the parameters of all the model equations, fatigue life prediction was made by making additional assumptions and setting a failure criterion. The first assumption was that influence of σ on the damage degree of fiber causes the fiber breakage. The second assumption was $\sigma$is perpendicular to the fiber so there is no effect this is on the fiber breakage. So the matrix is under multi-axial state of stress. For the failure criterion, the authors used the unit value for damage coefficient for both fiber and matrix breakage.

Finally, experimental data and model data is presented with comparison and the error values, which showed good agreement. Experiments indicate that, at the same cyclic loading fatigue

lives decrease as the angle of the fiber axis increases. The failure behaviors also follow in a similar fashion which is after matrix failure, fiber failure has occurred.

Owen and Howe [15] presented another damage model. According to the authors, fatigue damage in chopped strand matrix polymer is non-linear and stress independent. Miner rule cannot be applied for chopped strand composite due to non-linearity. They represented an equation for fatigue:

$$\Delta = \sum\{ B \left(\frac{n_i}{N_i} \right) - C \left(\frac{n_i}{N_i} \right)^2 \} \qquad \text{Eqn (2.16)}$$

Here, Δ is 1 at failure. n_i And N_i are the number of cycles endured and the number of cycles to failure, respectively.

2.1.11 Empirical Model

Epaarachchi and Clausen [16] presented an empirical model for various test frequencies and stress ratios in fatigue. For a specific composite this model needs a large amount of experimental data. Final model glass fiber composite is below

$$\left(\frac{\sigma_u}{\sigma_{max}} - 1 \right) \left(\frac{\sigma_u}{\sigma_{max}} \right)^{0.6\text{-}\acute{\eta}|\sin\theta|} \frac{1}{(1-\emptyset)^{1.6-\acute{\eta}\sin\theta}} f^{\,=\infty*(N-1)} \qquad \text{Eqn (2.17)}$$

A single graph can be drawn for a material irrespective of stress ratio, R, and test frequencies, f.

2.1.12 Slaughter Model

The compressive strength of fiber reinforced composites is relatively low; the value of compressive strength is sometimes less than 60% of tensile strength. This failure mechanism under compressive loading in polymer composites is called micro-buckling and occurs not only static loading but also in fatigue. Slaughter and Fleck presented a theoretical model [20, 21] which describes compressive fatigue micro-buckling.

The authors presented their model for monotonic compressive loading for fiber composite. They assume that a structure has developed imperfections during manufacturing due to initial misalignment of the fiber. This band of misaligned fibers is responsible for the micro-buckling. This misalignment is called a kink band angle, denoted by β in Figure [2.3]. Kink band angle is measured from the direction normal to the fiber and has a width w. $\overline{\varphi}$stands for initial kink band. After summing all the forces in ϵ_2 direction, following Eqn (2.18) is obtained.

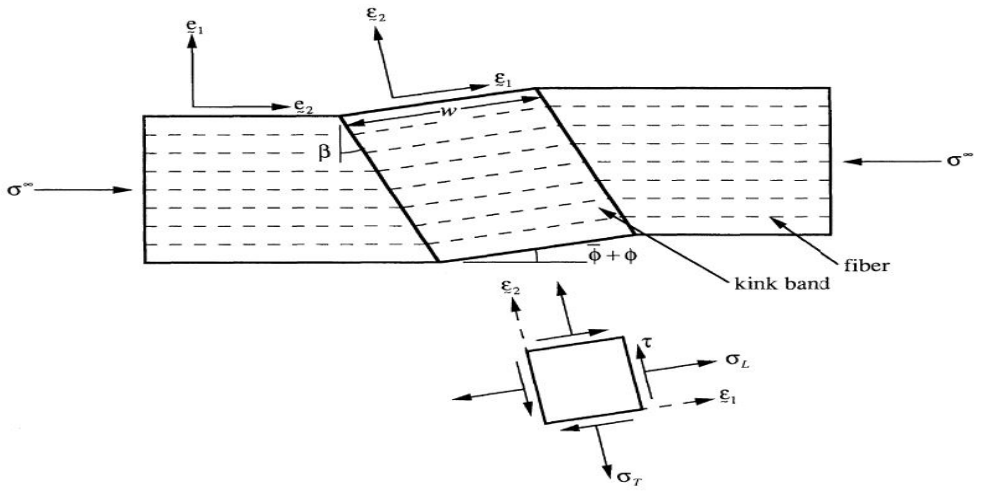

Figure 2. 3: Kink band geometry and notation [21]

$$\sigma^{\infty}\cos\beta\sin(\overline{\varphi}+\varphi)=\tau\cos(\beta-\overline{\varphi}-\varphi)+\sigma_T\sin(\beta-\overline{\varphi}-\varphi) \quad \text{Eqn (2.18)}$$

where, σ^{∞} stands for pure axial compression, τ stands for shear stress in $\underset{\sim}{\epsilon}_1-\underset{\sim}{\epsilon}_2$ coordinate system, σ_T is normal stress in the 2 direction. Assuming $\overline{\varphi},\varphi$ are very small we can write

$$\sigma^{\infty} \approx \frac{\tau+\sigma_T \tan\beta}{\overline{\varphi}+\varphi}$$ Eqn (2.19)

$$\gamma \approx \emptyset$$ Eqn (2.20)

According to Budiansky and Fleck, critical micro-buckling stress can be evaluated by previous Eqn (2.20). Assuming quadratic yield criteria,

$$(\tau/\tau_y)^2+(\sigma_t/\sigma_{ty})^2 = 1$$ Eqn (1.21)

where, τ_y and σ_{ty} are the plain strain yield stresses in pure shear and pure transverse tension, respectively. τ and σ_t are the applied stress in shear and transverse direction, respectively.

Now a new parameter is introduced, $R= \sigma_{Ty}/\tau_y$which stands for eccentricity of the yield ellipse. Plastic strain rates and plastic shear strain are expressed in terms of effective shear stress. The effective plastic strain is defined:

$$E_T/G=R^2$$ Eqn (2.22)

$$\gamma = \tau/G_s\tau_e$$ Eqn (2.23)

$$\gamma_e=\alpha\emptyset$$ Eqn (2.24)

$$\gamma_y = \tau_y/G$$ Eqn (2.25)

where,

$$\alpha = \sqrt{1 + R^2 tan^2\beta}$$ Eqn (2.26)

From the equation of pure shear, $\gamma_y = \tau_y/G$, equation (A) can be written as following

$$S^{\infty} = \frac{t}{\overline{\omega}+\eta} \qquad \text{Eqn (2.27)}$$

where, $S^{\infty} = \sigma^{\infty}/G^{*}$, $t = \tau_e/\tau_y$, $\eta = \gamma_e/\gamma_y$ and $\overline{\omega} = \overline{\varphi}/\gamma_y^{*}$.

$$\begin{cases} G^{*} = \alpha^2 G \\ \gamma_y^{*} = \gamma_y/\alpha \end{cases} \qquad \text{Eqn (2.28)}$$

Batdrof and Ko (1987) suggested and Budiansky and Fleck developed a Considere diagram that can be drawn like below on behalf of Eqn (2.27) where $\eta = {}^{G}/_{G_s}\, t$

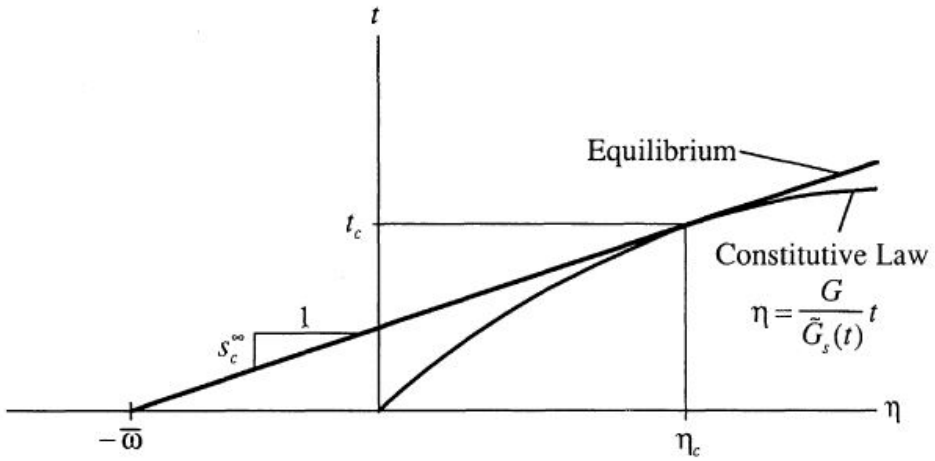

Figure 2. 4: Graphical representation for calculating critical micro-buckling stress under monotonic loading [21]

From Figure [2.4], Eqn (2.29) can presented

$$\left.\begin{array}{c} t_c = \left[\frac{7\bar{\omega}}{3(n-1)}\right]^{1/n} \\ S_c^{\infty} = \frac{1}{1+n\left(\frac{3}{7}\right)^{1/n}\left(\frac{\bar{\omega}}{n-1}\right)^{(n-1)/n}} \end{array}\right\} \qquad \text{Eqn (2.29)}$$

where n is the material parameter, t_c is strain component and S_c^{∞} is stress component.

During a compression-compression loading cycle, first the initial load is increased to S_{max}^{∞} then it is decreased to S_{min}^{∞}. Here $R = S_{min}^{\infty}/S_{max}^{\infty}$. Figure [1.5] represents the loading cycle.

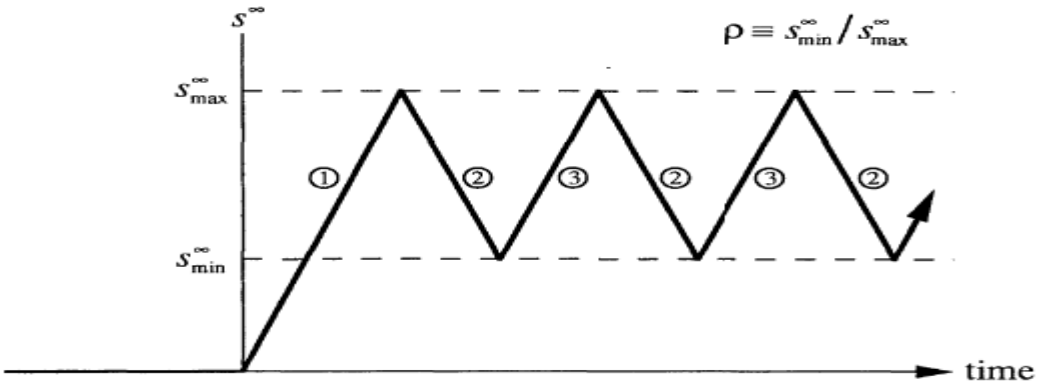

Figure 2. 5: Fatigue loading history [21]

Effective stress and strain, t and η, can be determined as a function of S^{∞} at the initial loading phase. Peak stress and strain, t_2 and η_2, correspond to S_{max}^{∞}. Figure [2.6] represents the king band stress strain history.

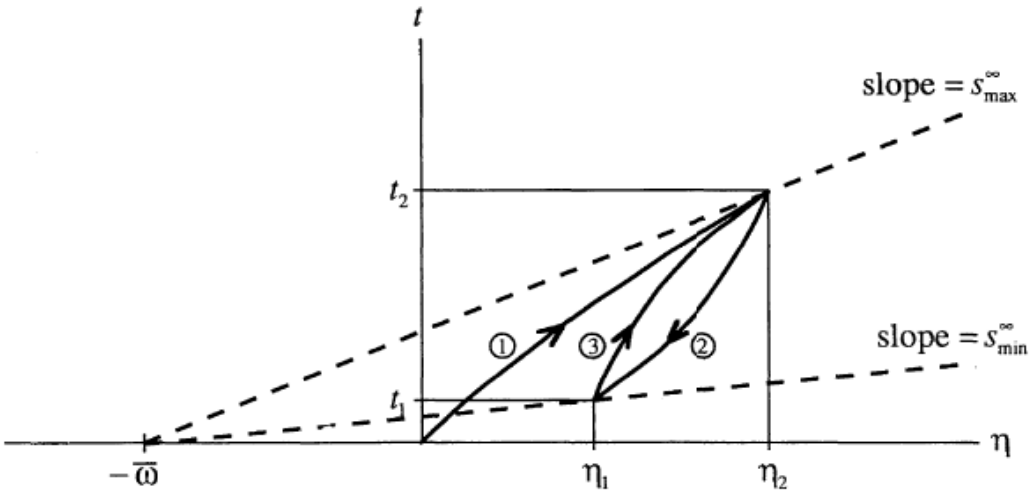

Figure 2.6: Stress- strain history with kink band

When load is reduced from maximum to minimum, the Mroz multi-yield surface hardening rule can be used to determine the composite constitutive behavior. Eqn (2.30) can be used to determine the effective stress in the kink band during unloading phase:

$$\eta = \eta_2 - \frac{2G}{\widehat{G(t_2-t)/2}}((t_2 - t) \qquad \text{Eqn (2.30)}$$

Using Eqn (2.30) for minimum and maximum stress, the difference between these two values are calculated. Using Eqn (2.31), the difference in effective strain also can be determined from the difference in effective stress.

$$\Delta\eta = \frac{6}{7}(\Delta t/2)^n \qquad \text{Eqn (2.31)}$$

$\Delta\eta^p$ can be found in terms of s^{∞}_{max}, s^{∞}_{min}, $\overline{\omega}$ and n. The following equations are solved for root.

$$t_2 - S^{\infty}_{max}\left(t_2 + \frac{3}{7}t_2^n + \bar{\omega}\right) = 0 \qquad \text{Eqn (2.32)}$$

$$\Delta t - \left(1 - \frac{S^{\infty}_{min}}{S^{\infty}_{max}}\right)t_2 + S^{\infty}_{min}\left(\Delta t + \frac{6}{7}(\Delta t)^n + \bar{\omega}\right) = 0 \quad ( ) \qquad \text{Eqn (2.33)}$$

As the power of this equation is n, so there is n no solutions, but among them smallest positive real solutions is our interests. After solving the other parameters we can find the no of cycle for particular stress condition by the following equation.

$$\frac{\Delta\eta}{2} = \frac{\gamma_f'}{y_y}(2N_f)^c \qquad \text{Eqn (2.34)}$$

In this paper there are remaining two chapters. Materials were test methods were discussed in second chapter including brief description. Third chapter is belonging to results and discussion with test data and analysis. Besides the S-N curve stiffness degradation analysis, adequate model fit and image processing analysis with appropriate image has been discussed.

CHAPTER THREE: MATERIALS, TEST METHODS and ANALYSIS

3.1 Materials

To conduct this study, E-glass fiber and polyester resin were used. Reinforcement and matrix materials were supplied by LM Windpower. LM Windpower is a leading wind turbine manufacturer. Unidirectional E-glass fibers were used in this research. Chopped strand fibers were attached to one side of the fiber sheet. The amount of chopped strand is approximately 6% of total fiber by weight [18]. Table [3.1] represents the properties of fibers.

Table 3.1: Properties of E-Glass fiber [18]

E-Glass Fiber		
Property	Value	Unit
Tensile Strength	1700-3500	MPa
Density	2490	kg/m^3
Modulus	73	GPa
Shear Modulus	30	GPa
Poisson's Ratio	0.23	

Resin used here was POLYLITE® 413-575 The properties are in Table [3.2] given below.

Table 3. 2: Properties of POLYLITE® 413-575 [18]

POLYLITE® 413-575		
Property	Value	Unit
Tensile Strength	40-90	MPa
Compressive Strength	90-250	MPa
Shear Strength	45	MPa
Density	1100-1500	kg/m^3
Modulus	3.2-3.5	GPa
Shear Modulus	0.7-2.0	GPa
Poisson's Ratio	0.3-0.35	

3.2 Plate Fabrication

For this study, plates were fabricated by Vacuum Assisted Resin Transfer Molding (VARTM). Details the fabrication process are in below. Figure [3.1] shows the E-glass fibers.

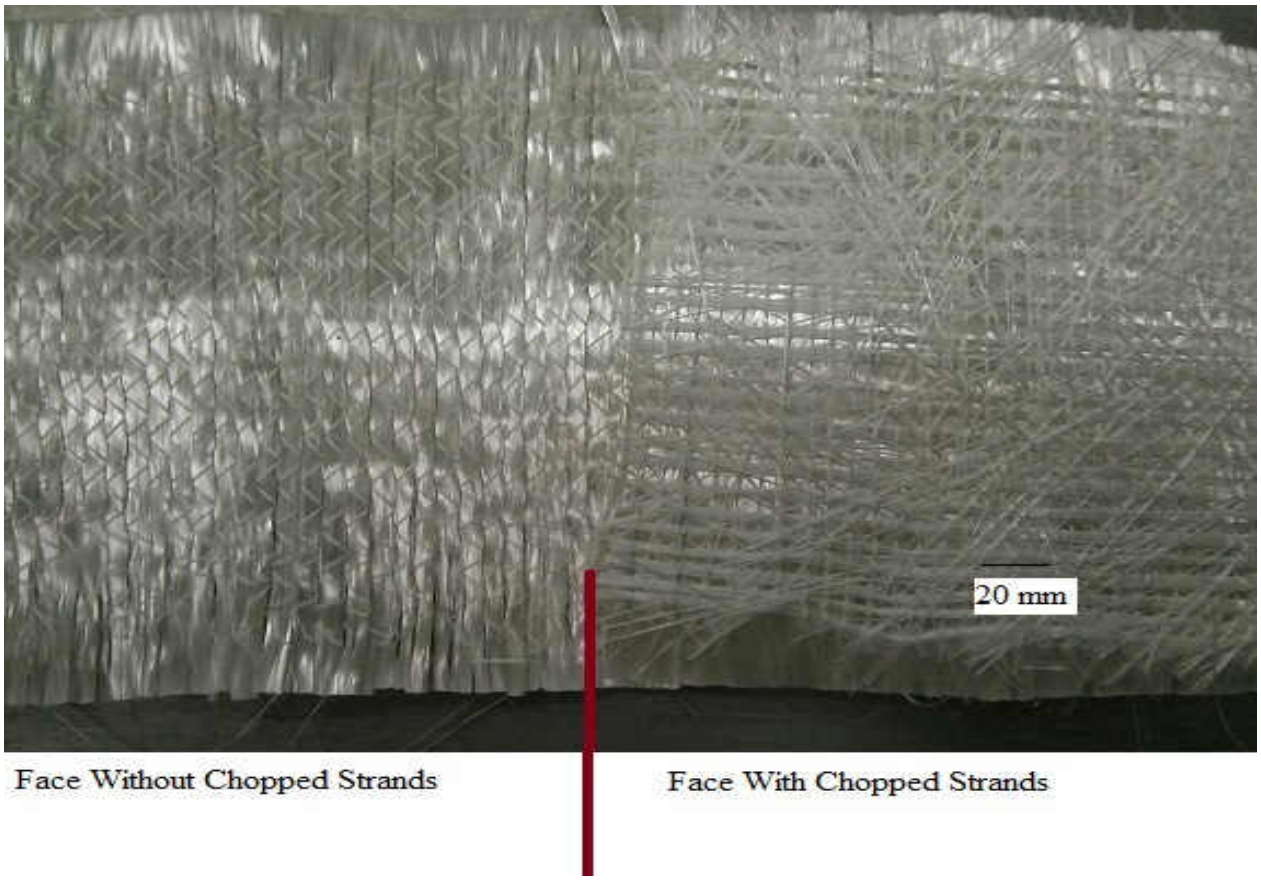

Figure 3.1: Images of fiber reinforced used during this study

There are two faces of fiber in the Figure [3.1]. Left side of the red marking represents clean surface and right side represents surface with chopped strands. The reason of name termed as clean surface is this surface is free of chopped strands.

Figure [3.2] shows the supporting materials for making plate.

Figure 3. 2: Supporting materials for vacuum bagging

3.3 Steps in manufacturing process

- Clean the metal work surface.
- Place two sided sealing tape at the approximate boundary of vacuum bagging.
- Apply release agent (wax) to work surface.
- Stack fiber. At the mid-plane clean side were facing each other.

Figure [3.3] shows the drawn diagram for 10 layers lay-up of fibers.

Figure 3. 3: Sequential lay-up of 10 layers plies.

- After stacking 10 layers of fibers, peel ply was placed above them.
- Square perforated plates were placed above the peel ply.
- Breather ply was placed above the rectangular plate.

Figure [3.4] shows the sequential lay-up of supporting materials with fibers.

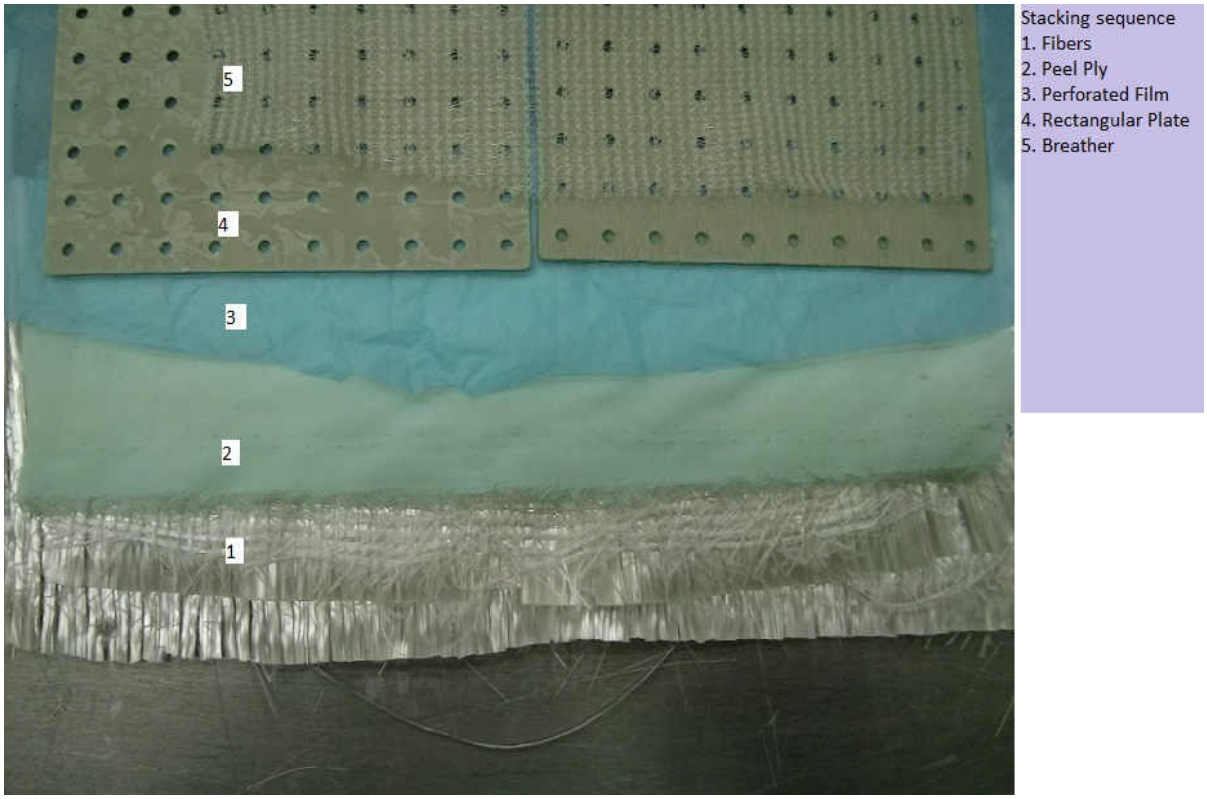

Figure 3. 4: Sequential lay-up of all supporting materials with fibers

- Spiral tube was attached with suction tube of resin and the spiral tube was placed above the breather.
- Another spiral tube was attached to the resin exhaust tube below the peel ply and above a two sided tape.
- Plastic vacuum bagging was placed in a fashion that four wrinkles will be necessary. To make wrinkles four extra identical vertical sealing tape was attached in flat tape.
- Inlet tube was bent and taped to make airtight. Outlet tube was attached with resin collector which was attached with the vacuum pump.

- Vacuum pump was started then to check the pressure. It is required to maintain (-) 27 kPa. Need to locate out any potential leaks that will cause a reduction in vacuum level.
- After confirming the vacuum pressures, resin infusion can be started.

3.3.1 Resin Infusion

- Weigh a plastic pot with stirrer.
- Pour approximate quantity of resin in that pot (W1).
- Weigh again the pot with resin (W2).
- Subtract the 1st weight from 2nd one (W3=W2-W1).
- Calculate 1.5% of subtracted value (W4=1.5%of W3).
- Calculate the display value of pot+ resin+ stirrer+ desired initiator (W5=W4+W2).
- Slowly pour initiator into the resin; if needed, use dropper.
- Write down the time immediately after pouring initiator.
- Mix properly, alternating clockwise and anticlockwise; make 8 CW and make 8 CCW. All the steps should be done minimum 30 sec
- Place the pot with mixture (Top surface of the mixture need to be at 16-20 cm below from the surface of the metal plate in which fiber is placed).
- Bend the inlet pipe properly then dip into the resin. Make sure no air bubble are going into the pipe (if needed, use tape to bend the pipe).
- Unbend the pipe and vacuum infusion will start.
- Check with eye that is there are not any bubbles coming from any side of the taping.
- Wait for resin to reach the vacuum side spiral tube at all points.

- Reduce the pressure 30%.
- After 10 min, cut off the resin transfer.
- Wait for curing 24 hr (standard time).
- Remove the plate from the vacuum bagging; place in oven at 65°C for 14 hr (post -cure).

3.4 Test Sample Preparation

After room temperature curing and post-curing, test samples were cut from the plate. Approximately 15-18 samples can obtained from 610 mm wide plate. According to ASTM D6272 [25] standard dimensions of each sample 203.2 mm x 25.4 mm x thickness. The plate was cut to the dimension: 254 mm x 25.4mm x thickness. The extra portion have taken in the longitudinal direction to keep some extra portion outside of support span. Cutting was done by table saw and marked instantly. A diamond saw blade was used for cutting.

3.5 Hardness Test Result

After cutting all the samples, hardness was measured by shore hardness tester manufactured by CheckLine. The name of this equipment is DD-100. The resolution of this machine is 0.1. Hardness data are in Appendix A. The average value of the hardness for plate A is 89.1, for plate B is 88.2 and for plate D is 88.4.

3.6 Static Test

Static 4-point bending tests were performed using a 50-kN SHIMADZU AG-IS universal testing machine. Figure [3.5] shows the free body diagram of 4-point bend test.

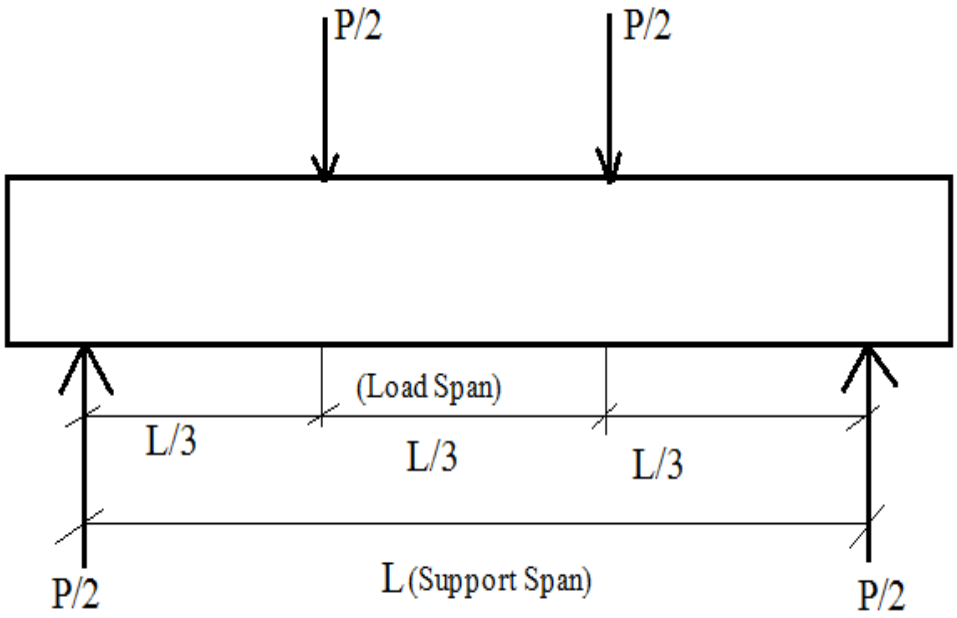

Figure 3. 5: Free body diagram of 4-point bend test

here,

- P= Load
- L= Acting length (Support Span) of the beam

For both static and fatigue, L can be chosen. In this study, L was taken as 203.2 mm. Load span was taken here one third of support span. The test was conducted under displacement control; applied load was monitored. The crosshead speed varied sample to sample and was calculated by using Eqn (3.1) from the ASTM D6272 [25].

$$R=0.185ZL^2/d \qquad \text{Eqn (3.1)}$$

here,

- R= rate of crosshead motion [mm/ min]
- L= support span [mm]
- d= depth of beam [mm]
- Z=0.01

To calculate the strength of the composite, Eqn [3.2] was used. This equation is valid when the support span to depth rations greater than 16.

$$S = (PL/bd^2)[1 + 4.70(D^2/L^2) - (7.04Dd/L^2)] \quad \text{Eqn (3.2)}$$

Here,

- B = width of beam [mm]
- D = Maximum deflection of the center of the beam [mm]

3.7 Fatigue Test

Fatigue testing was performed using a Bose Electroforce 3510 testing machine. The theoretical capacity of that machine is 7.5 kN. But this depends on the average applied load: heat generated by the magnetic actuators reduces the actual capacity. For these tests, the maximum load capacity was set for 7.1kN. Figure [3.6] shows the experimental setup for the fatigue test.

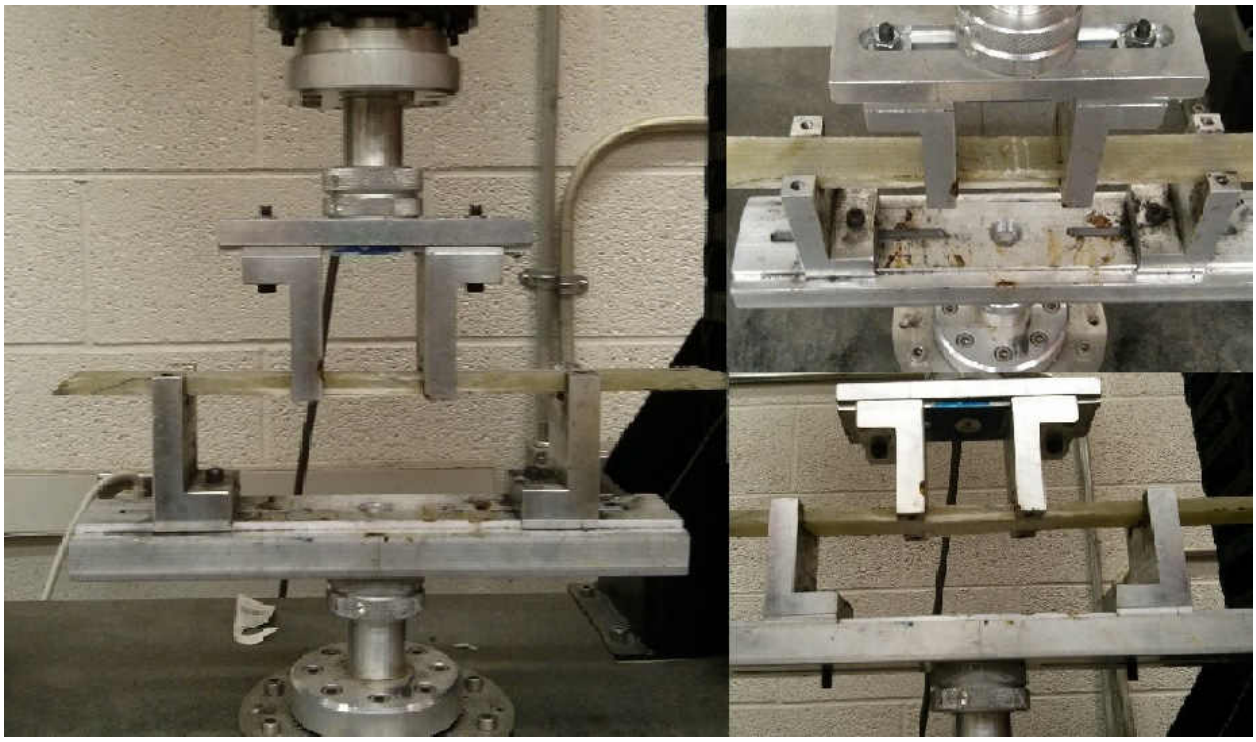

Figure 3. 6: Pictorial view of fatigue test set-up.

This jig is only applicable for a positive load ratio. It is not able to pull the sample upwards.

Load Ratio, R = Minimum Load/Maximum Load Eqn (3.3).

Prior to fatigue testing, the control parameters must be identified (i.e. the system must be tuned). Samples were placed in the jig with proper way. Load control was specified and sinusoidal loading curve was chosen. The Tune IQ function was used to determine the PID control settings.

3.8 Determination of Volume Fraction

After conducting fatigue tests, volume fraction of fiber of each plate have determined according to ASTMD3171 [24]. A thin portion was cut from the samples to conduct the burn off test. The approximate dimension was for the thin portion was 6 mm x 25.4 mm x thickness of each

sample. A water filled test-tube was used to measure the volume of samples. Samples were placed in the test-tube and the increasing in volume was measured. Then mass of each sample and the mass of crucible was measured. The samples were placed in the oven for four hours at 600°C to burn off all the resin. After cooling the crucible the mass of the remaining fibers was measured. Finally, Eqn [3.4] was used to calculate the fiber volume fraction of each sample.

$$V.F = (M_{fiber}/M_{comp})*100*(Density_{comp}/Density_{fiber}) \quad \text{Eqn (3.4)}$$

Table [3.3] shows the average fiber volume fraction of each plate.

Table 3. 3: Fiber volume fraction results

Plate	Volume Fraction
A	59.4 ± 0.44
B	56.4 ± 0.78
D	55.8 ± 2.31
Overall Mean	57.22 ± 2.065

Fiber volume fraction is a properties that depends on the manufacturing process. Hand layup and VARTM process gives different values of volume fraction of fiber. Sadeghian et al [23] stated in their article that they found 43% volume fraction for the glass fiber composite by VARTM process. Reimbayev, M. [18] did similar type of study with similar material as this study. He found around 58.9% fiber volume fraction of 8 layers of plate with the VARTM process.

3.9 Stiffness Degradation Analysis

When a beam deforms under fatigue loading, deflection of that beam increases as the no of cycle increases. That means the stiffness of the beam decreases with the increasing no of cycle. In this work, stiffness degradation of every sample has calculated and then plotted them in a same

fashion to find any co relation. Following figure represents the free body diagram of four point bending tests that was used here.

To find the stiffness following Eqn [3.5] is used [9].

$$E_{bend} = P*a* (4a^2-3L^2)/(48DI) \qquad \text{Eqn (3.5)}$$

All of the parameters of above equation are constant for a particular sample without load, P and deflection, D. These two parameters can be found from the data file that was stored in the computer connected with fatigue test machine. At every hundred cycle of a fatigue test computer stored load and deflection data for that particular cycle in a file. With this data and from above equation, stiffness of every hundred cycle has calculated. After normalizing the stiffness and no of cycle, they are plotted. Plotting details is in result and discussion section.

3.10 Image processing

When a sample fails in fatigue test, it observed fracture in it's surface. Sometime fracture occurs only in compression or tension surface, sometimes in both surfaces. To quantify this surface fracture in both surface and finding a relation with maximum applied stress or any other factor, image processing of failed samples has done. To perform the image processing picture was taken for all the samples in an isolated condition. Isolation means here same lighting, same distance from surface, same angle of camera. After getting picture of every sample in a same fashion, they processed in Image J software. But to perform various level of thresh holding and also making compare with other software, Matlab function was used. All of data are presented in result section to show the co relation. An image is transferred to gray picture from RGB picture. When it was converted in gray form, all the pixels are marked in 20 to 200 numerical value of color range. Then for thresh holding application the algorithm is select a numerical value of color between the previous range. The this value has applied in such a way that, below this value all

the pixels are converted to black region and above this value all the pixels are converted to white region.

3.11 Failure or stopping Criteria

The stopping criteria of each fatigue test in this study are chosen maximum life-time and maximum crosshead displacement. Maximum infinite life-time was 2 million cycle for this study. That means the test topped after reaching the two millions cycles for a particular sample if that sample was not failed. But those samples were failed before two million cycles, the stopping criteria for those sample were maximum displacement. The maximum displacement was 23 mm. The reason of choosing 23mm as limit of maximum displacement is that in the static test all the samples failed before 22mm.

CHAPTER FOUR: RESULTS AND DISCUSSIONS

4.1 Static Test Result

Five samples from single plate were tested statically under the procedure of ASTM standard D6272 [25]. The test method was 4 point static bending test. According to the standard all coupons were cut 254-280 mm long parallel to the fibers and 25.4 mm wide in the transverse direction. The support span was used as 203.2 mm and load span was one third of support span. After measuring all the dimensions of a particular sample, the crosshead rate was calculated using Eqn (3.1). Load and crosshead displacement were captured during the test. Maximum fiber stress and maximum strain were calculated according to Eqn (3.2) and Eqn (3.3), respectively. The Table [4.1] shows the calculated data for every sample in static testing.

Table 4. 1: Static test result

Sample Name	Width (mm)	Depth (mm)	Rate of Cross Head, R (mm/min)	Deflection At max load, D (mm)	Strain (mm/mm)	Maximum Fiber Stress, S (MPa)
A3	25.1	8.44	9.05	19.5	.019	769
A6	25.28	8.51	8.978	22.21	.022	821
A9	25.63	8.54	8.941	20.52	.02	792
A12	25.75	8.56	9.923	20.53	.02	781
A15	25.72	8.5	8.986	20.67	.021	790
Average						790.6
Standard Deviation						19.27

The average flexural strength was determined to be 790.6 MPa with the standard deviation of 19.3 MPa. Figure [4.1] shows the applied force vs displacement of the samples. It can be seen that the behavior of every sample in static test was similar. All samples failed by buckling/delamination on the compressive surface of the beam.

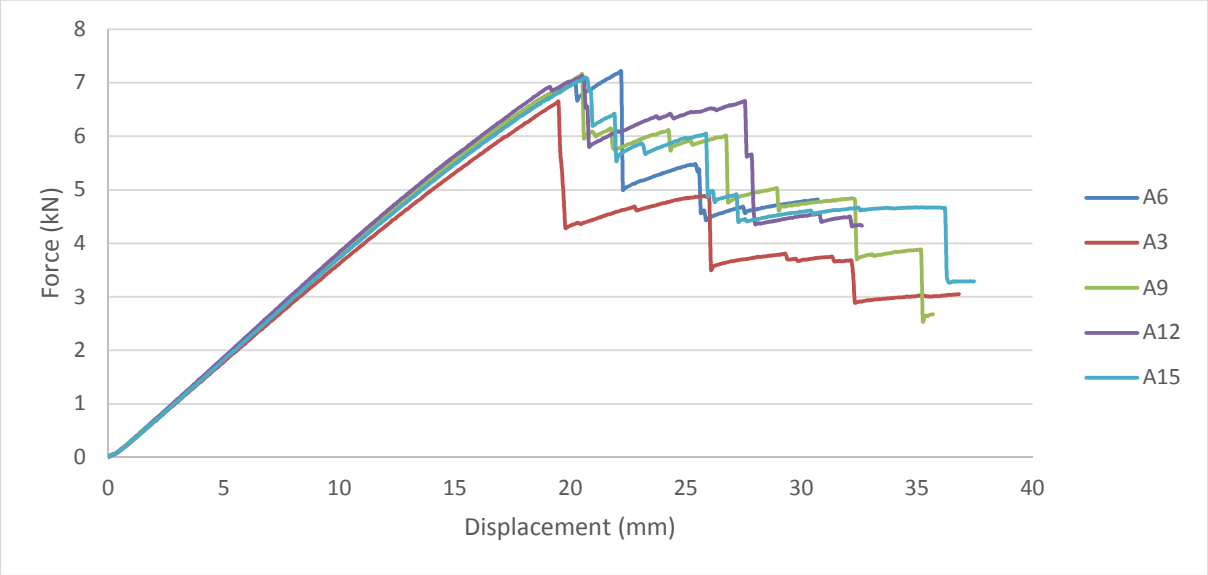

Figure 4. 1: Force (kN) vs Displacement (mm) graph of static testing

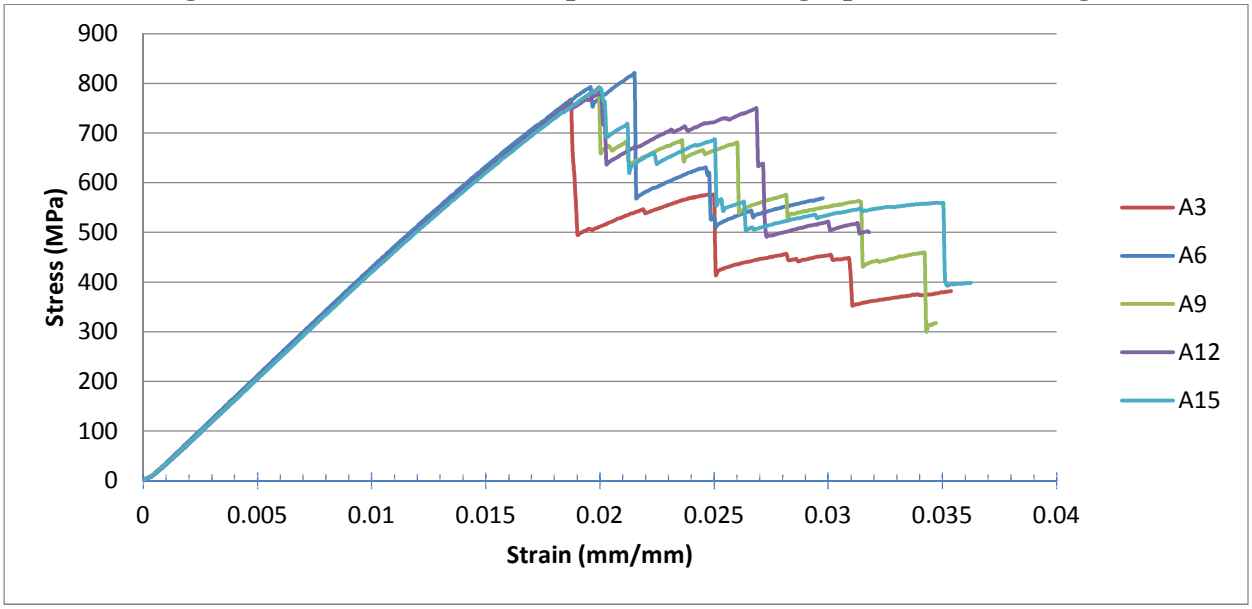

Figure 4. 2: Stress (MPa) vs Strain (mm/mm) of static testing.

Figure [4.2] shows the relationship between the stress and strain of each sample.

Flexural modulus /slope have been calculated from this curve.

$$\text{Flexural modulus} = \frac{Stress_1 - Stress_2}{Strain_1 - Strain_2} = \frac{600-300}{.0145-.0072} = 4.1 \text{ GPa}$$

Figures [4.3-4.4] show the images of the compressive and tensile faces of the specimens.

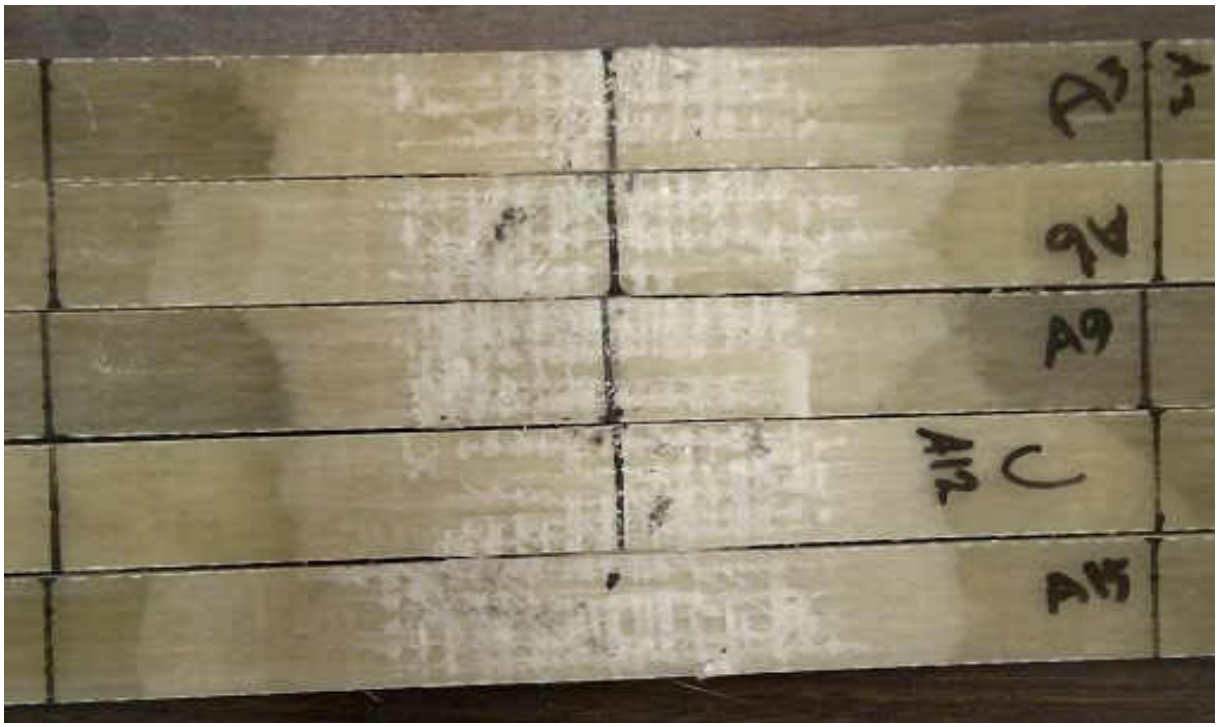

Figure 4. 3: Compression surface of failed samples from static test

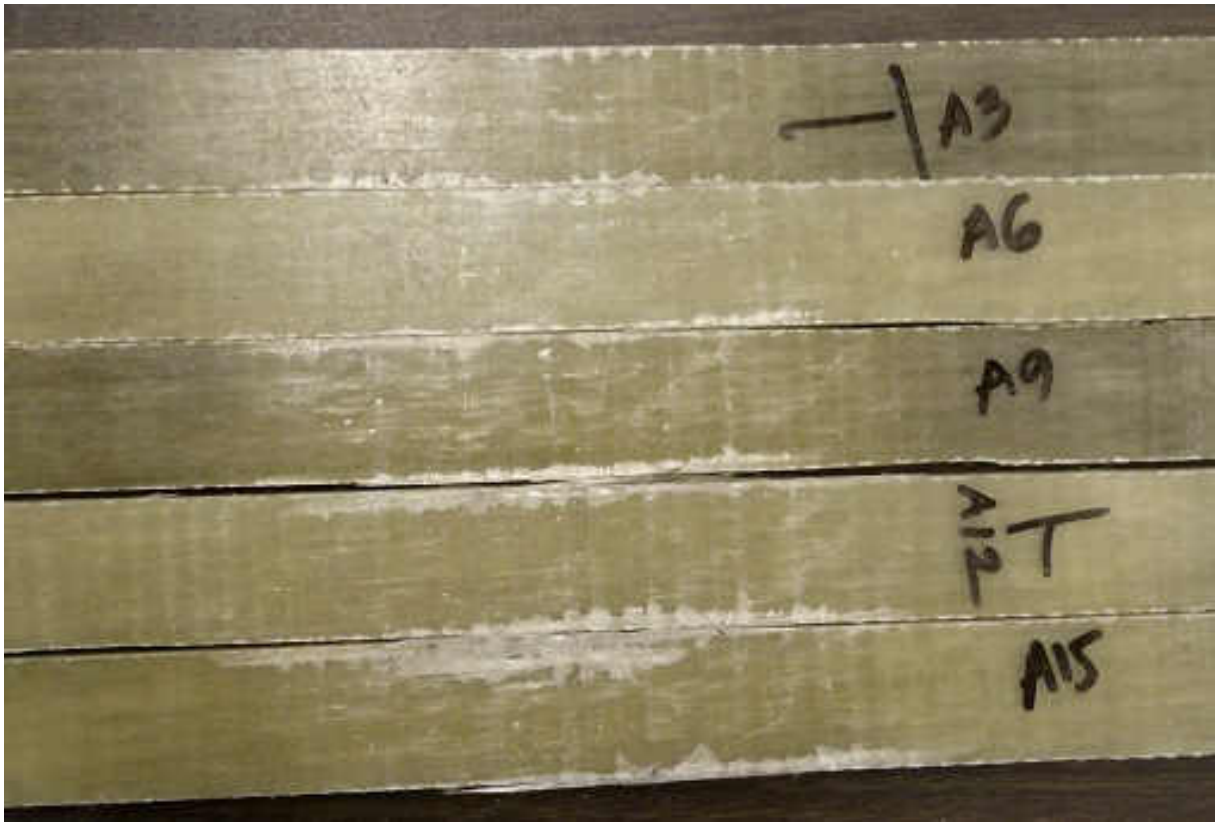

Figure 4. 4: Tension surface of failed samples from static test

All samples from Figure [4.3] shows the failure is in compression. On the other hand, all samples of Figure [4.4] show only little edge fracture in tension surface. But the edge fracture in last sample is slightly bigger than other four.

4.2 Fatigue Test Result

After determining the maximum average strength from static testing, fatigue testing was started. Various values of stress ratio, R, were chosen for the fatigue testing. Here,

R= (Min Stress)/ (Max Stress) Eqn (4.1)

R=0.1, 0.3, 0.5, 0.7 for these tests. Dimensions of fatigue samples were the same as for static testing. The maximum applied fatigue load was approximately 90% of the maximum static load.

Then maximum applied load was decreased as R was held constant to create an S-N plot for each value of R. Tests were conducted under the load control and failure criteria was defined by two conditions. One is displacement of the load span which is same for the test coupon. The value of the maximum displacement was given to 22 mm. Decision was made from the observation of static test. The second criteria was number of cycle in the test as 2 million. Table [4.2] shows the results of all fatigue tests.

Table 4. 2: Fatigue Test Data

Load Ratio, R	Sample Name	Length, L (mm)	Thickness (mm)	Width (mm)	Maximum Stress (MPa)	Minimum Stress (MPa)	Cycles to failure
0.1	D14	203.2	8.83	25.82	666.2	66.6	540
	D2	203.2	8.87	25.82	600.2	60.0	1502
	D10	203.2	8.66	25.84	576.7	57.7	13809
	D17	203.2	8.69	25.40	529.7	53.0	33630
	D12	203.2	8.68	25.51	475.7	47.6	108390
	D13	203.2	8.73	25.53	365.5	36.6	594720
	D18	203.2	8.69	25.88	259.9	26.0	2000002
0.3	A13	203.2	8.54	25.76	711.0	213.3	76
	A7	203.2	8.57	25.60	702.5	210.7	852
	A16	203.2	8.56	25.54	651.5	195.4	4736
	A18	203.2	8.52	25.51	603.5	181.1	13772

	A8	203.2	8.55	25.60	542.9	162.9	43323
	A17	203.2	8.50	25.60	494.4	148.3	44248
	A11	203.2	8.54	25.57	381.4	114.4	583926
	A4	203.2	8.47	25.76	274.9	82.5	2000002
0.5	A5	203.2	8.64	25.69	699.3	349.7	192
	F3	203.2	8.55	25.59	675.4	337.7	2984
	B17	203.2	8.77	25.72	616.3	308.2	61773
	B18	203.2	8.76	25.72	566.2	283.2	88838
	B16	203.2	8.87	25.70	502.5	251.2	182779
	B13	203.2	8.87	25.70	452.2	226.1	614581
	B8	203.2	8.83	25.54	357.1	178.6	2000002
0.7	B6	203.2	8.84	24.62	697.1	488.0	3636
	A14	203.2	8.67	26.26	648.5	454.0	16317
	B11	203.2	8.90	25.74	598.0	418.6	48164
	B7	203.2	8.87	24.81	572.5	400.8	136019
	B14	203.2	8.91	25.66	498.7	349.1	706351
	B9	203.2	8.81	25.52	461.6	323.1	2000002

Sample, A17, is showing low life cycle from the other samples of R=0.3. An experiment was replicated at this condition that is in the end of this chapter.

Figure [4.5] shows the combined S-N curves for all ratios.

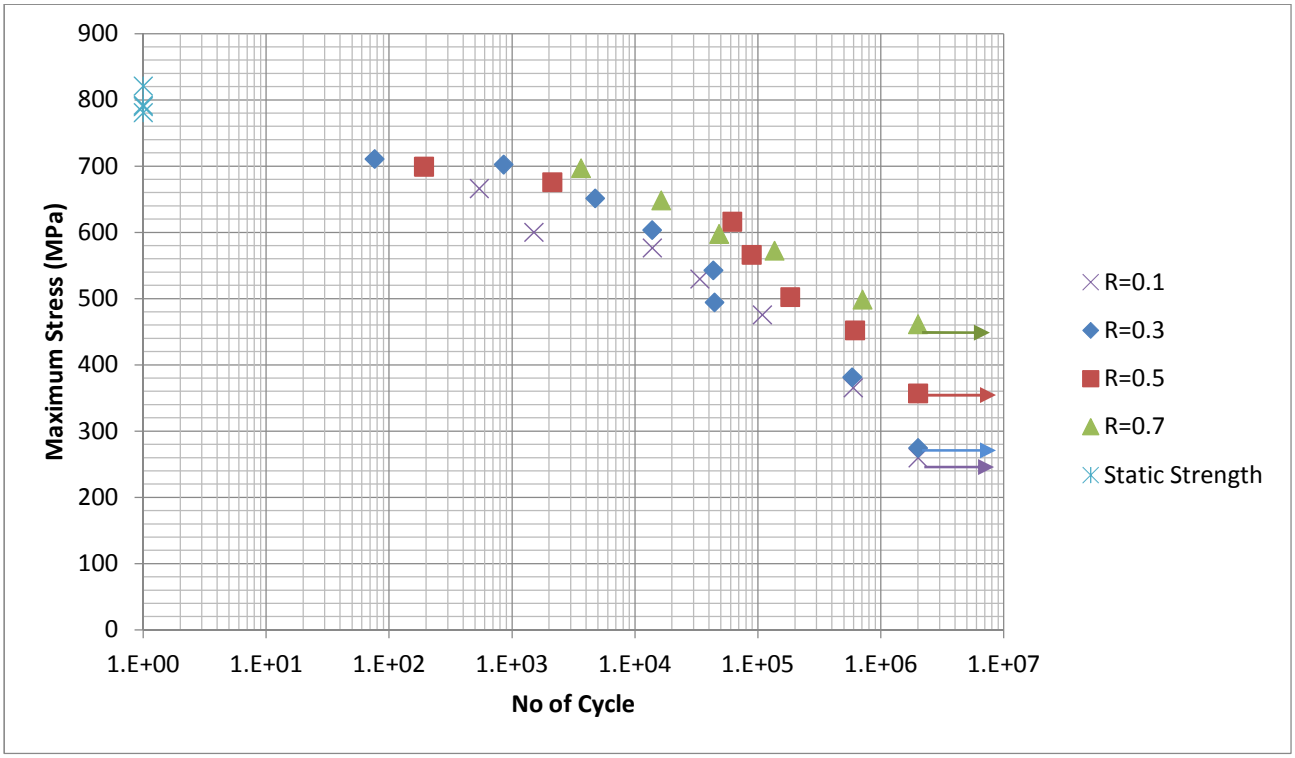

Figure 4. 5: S-N curve with static test result

Each value of R shows a similar form of S-N curve. Fatigue life at a given level of maximum stress is increasing with the increasing R. However, fatigue life difference between two ratios at a level of maximum stress is different in below than above of the 500 MPa. Above of the 500 MPa the difference is larger than the below. Furthermore, below of the 500 MPa, apparently there is no difference between the R value of 0.1 and 0.3. Finally, there is a difference in the sample of 600 MPa for R=0.1, which seems to be slightly out of place.

4.5 Modulus Degradation

Displacement and load data were stored throughout each fatigue test. An effective flexural modulus was calculated by Eqn (4.2).

$$E_f=P*a*(4a^2-3L^2)/(48DI) \qquad \text{Eqn (4.2)}$$

Here,

- P = Load
- L = Length of the beam
- a = Load Span= L/3
- D = Deflection
- I = Moment of Inertia

Figures [4.6-4.9] show the normalized flexural modulus vs normalized lifetime throughout the fatigue test for each sample. The normalized flexural modulus and lifetime are defined according to Eqn (4.3) and Eqn (4.4), respectively.

$$\text{Normalized instantaneous flexural modulus} = \frac{\text{fluxural modulus}}{\text{fluxural modulus at first cycle}} \qquad \text{Eqn (4.3)}$$

$$\text{Normalized lifetime} = \frac{\text{Number of cycles completed}}{\text{Number of cycles at failure}} \qquad \text{Eqn (4.4)}$$

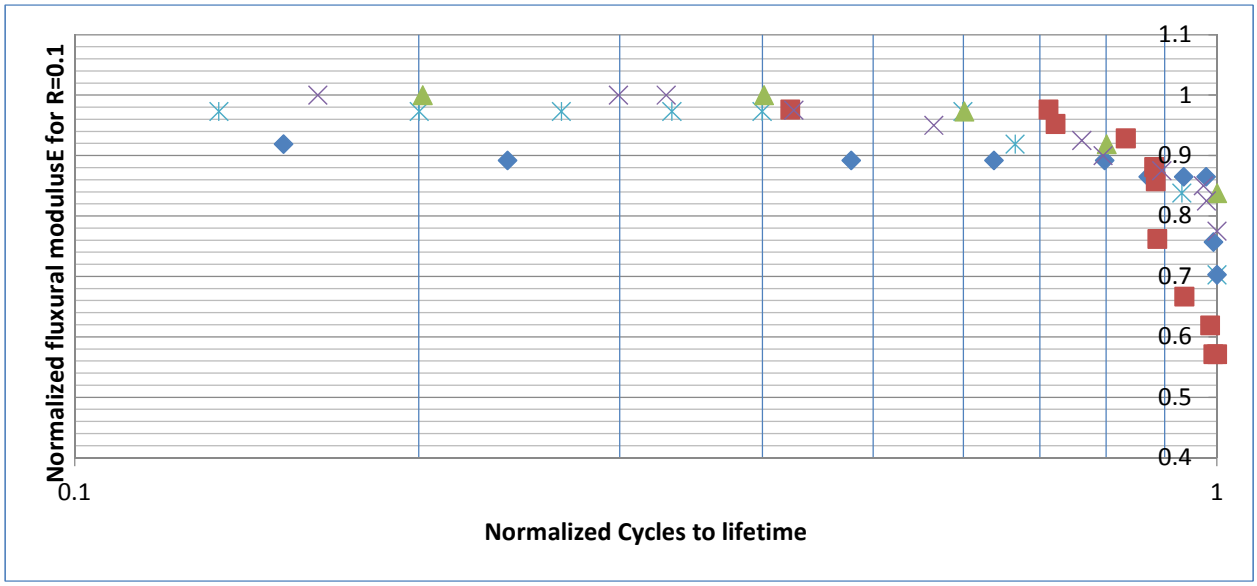

Figure 4. 6: Normalized flexural modulus vs normalized cycles to failure for R=0.1

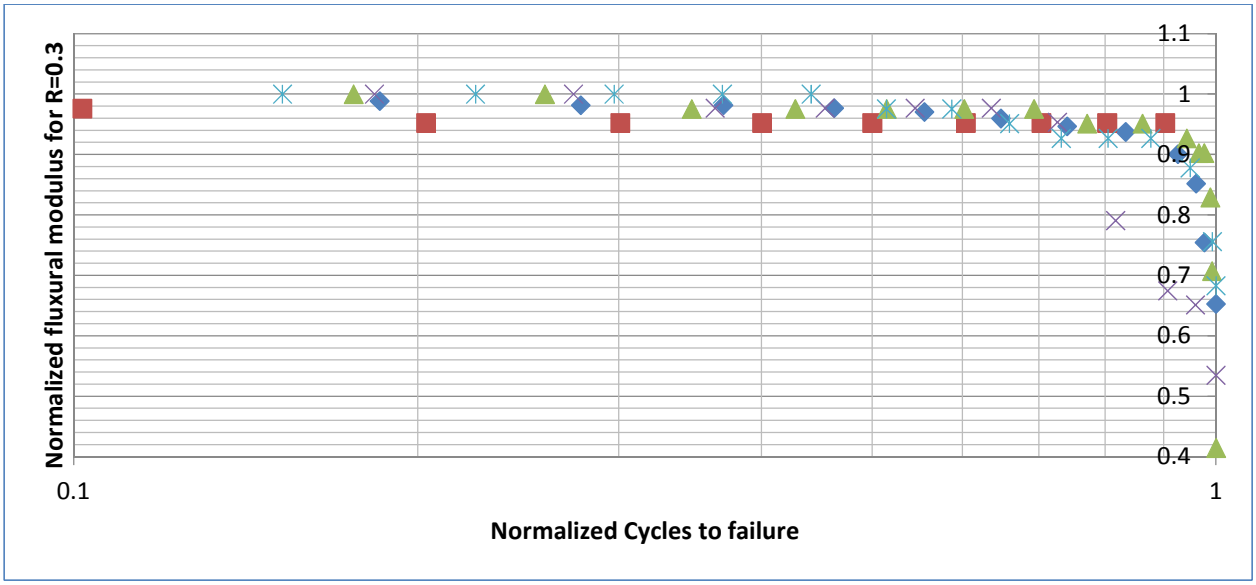

Figure 4. 7: Normalized flexural modulus vs normalized cycles to failure for R=0.3

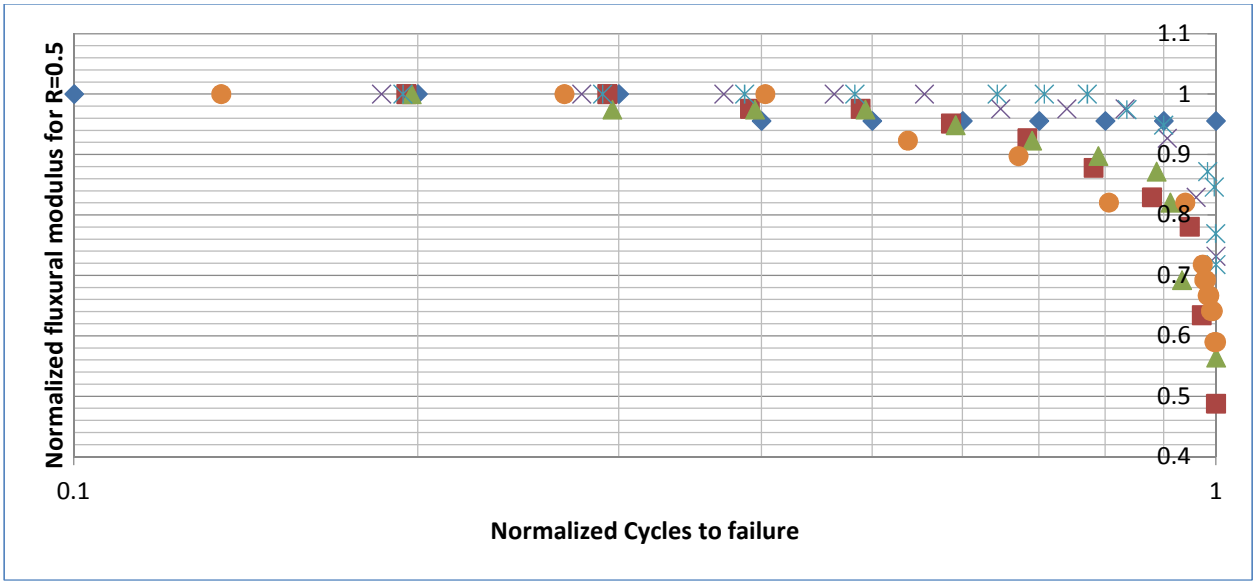

Figure 4.8: Normalized flexural modulus vs normalized cycles to failure for R=0.5

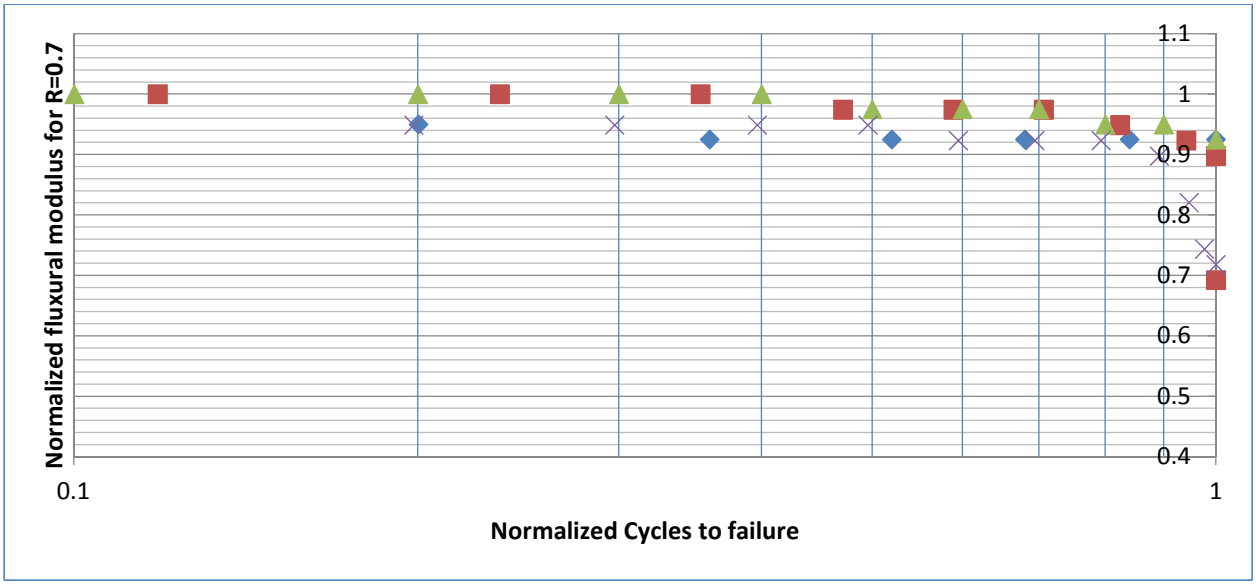

Figure 4. 9: Normalized flexural modulus vs normalized cycles to failure for R=0.7

It can be concluded that most of the degradation in the flexural modulus occurs after approximately 80%-85% of the fatigue life is completed for all values of R.

4.4 Model Fit Calculations

For the low cycle fatigue region the Slaughter-Fleck model has been used. The model description is presented in Chapter 1. The model parameters are presented the Table [4.3].

Table 4. 3: Parameters of Slaughter-Fleck model calculations.

Parameter	Value with Unit	Remarks
$\sigma_{\propto}$	792MPa	Maximum stress found from static test
σ_{Ty}	50MPa	[18]
tan(β)=tan(20)	0.364	[21]
Kink band angle	0.069778 radian	Initial Kink Band in radian (4˚)
τ_y	30.83 MPa	Experimental measurement
R	1.62	Eccentricity of the yield ellipse from

α	1.16	From Eqn (2.25)
G	2.93GPa	[18]
γ_y	0.0105	From Eqn (2.24)
G*	3.95	From Eqn (2.27)
γ_y^*	0.009	From Eqn (2.27)
S_c^*	0.2	From Eqn (2.28)
$\bar{\omega}$	7.7	From Eqn (2.26)
n	2.17	Root Solution of Eqn (2.28)

Using these values, model parameters were determined for all stress ratios. This procedure was also described in Chapter 1. Tables [4.4-4.6] and Figures [4.10-4.12] show the resulting models for R=0.1, 0.3 and 0.5. For R=0.7, $t_2$and Δt have no real solution. This is why there is no comparison with Slaughter-Fleck's model for R=0.7.

Table 4. 4: Calculated fatigue life of Slaughter's model for R=0.1

R=0.1						No of Cycles		
Max Stress (MPa)	S_{max}^{∞}	S_{min}^{∞}	t_2	Δt	$\Delta\eta$	Model 1 $c = .2$ $\frac{\gamma_f'}{y_y} = 1$	Model 2 $c = 0.3$ $\frac{\gamma_f'}{y_y} = 1$	Model 3 $c = 0.3$ $\frac{\gamma_f'}{y_y} = 2$

712.8	0.1804	0.0180	2.21	1.76	0.6520	136	21	211
705	0.1784	0.0178	2.15	1.72	0.6207	174	25	249
700	0.1772	0.0177	2.12	1.69	0.5978	210	28	282
690	0.1746	0.0175	2.05	1.64	0.5606	289	35	350
675	0.1708	0.0171	1.96	1.56	0.5037	494	50	500
625	0.1582	0.0158	1.7	1.36	0.3755	2143	132	1330
550	0.1392	0.0139	1.39	1.11	0.2431	18833	562	5663
500	0.1265	0.0127	1.2	0.96	0.1782	89037	1583	15952

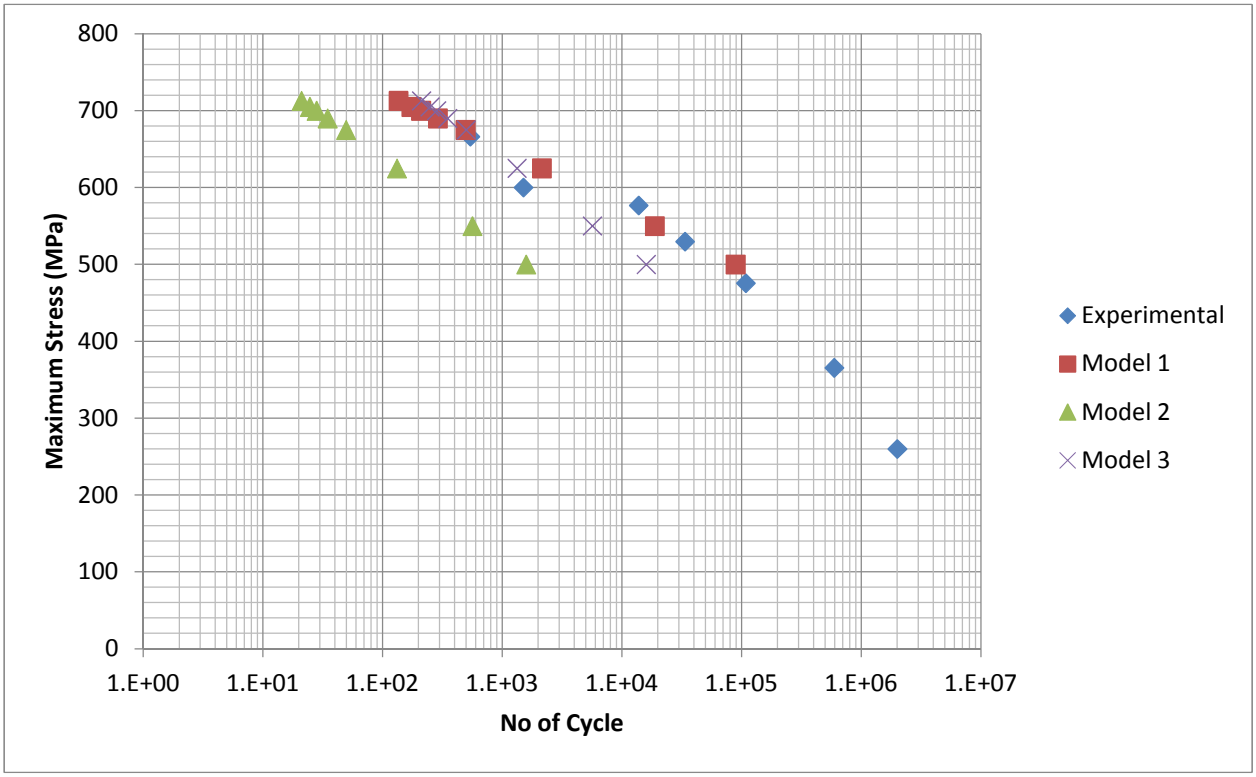

Figure 4. 10: Comparison of three model data with experimental data for R=0.1

In Figure [4.10] model 1 is matching properly with the experimental data. Only one point is slightly out of the curve. Also from the model adequacy analysis, model 1 is showing least error fit with the experimental data.

Table 4. 5: Calculated fatigue life of Slaughter's model for R=0.3

R=0.3						No of Cycles		
Max Stress (MPa))	S_{max}^{∞}	S_{min}^{∞}	t_2	Δt	$\Delta \eta$	Model 1 $c = .3$ $\frac{\gamma_f'}{y_y} = 1$	Model 2 $c = 0.6$ $\frac{\gamma_f'}{y_y} = 4$	Model 3 $c = .7$ $\frac{\gamma_f'}{y_y} = 15$
712.8	0.1804	0.0541	2.21	1.02	0.2029	1027	228	629
705	0.1784	0.0535	2.15	0.99	0.1903	1271	254	689
700	0.1772	0.0531	2.12	0.98	0.1862	1366	263	711
690	0.1746	0.0524	2.05	0.94	0.1704	1839	306	808
675	0.1708	0.0513	1.96	0.9	0.1552	2508	357	922
625	0.1582	0.0475	1.7	0.77	0.1112	7631	623	1486
550	0.1392	0.0418	1.39	0.61	0.0675	40199	1429	3029
500	0.1265	0.0380	1.2	0.52	0.0480	125531	2525	4935

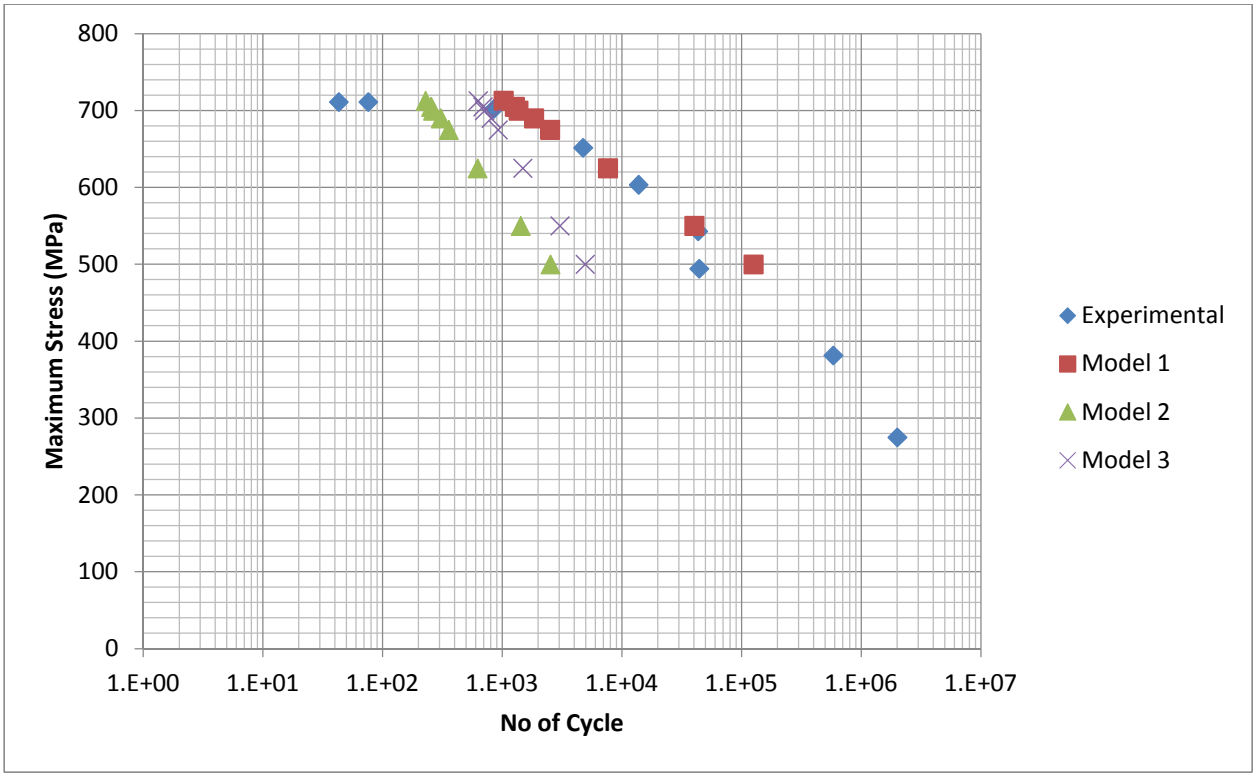

Figure 4. 11: Comparison of three model data with experimental data for R=0.3

In Figure [4.11] model 1 is matching properly with the experimental data. Only one point is slightly out of the curve. Also from the model adequacy analysis, model 1 is showing least error fit with the experimental data.

Table 4. 6: Calculated fatigue life of Slaughter's model for R=0.5

R=0.5						No of Cycles		
Max Stress (MPa)	S_{max}^{∞}	S_{min}^{∞}	t_2	Δt	$\Delta\eta$	Model 1 $c = .53$ $\frac{\gamma_f'}{y_y} = 1$	Model 2 $c = .9$ $\frac{\gamma_f'}{y_y} = 4$	Model 3 $c = .9$ $\frac{\gamma_f'}{y_y} = 20$

712.8	0.1804	0.0902	2.21	0.37	0.0232	2250	331	1977
705	0.1784	0.0892	2.15	0.35	0.0206	2816	377	2256
700	0.1772	0.0886	2.12	0.34	0.0193	3166	404	2417
690	0.1746	0.0873	2.05	0.32	0.0170	4044	467	2792
675	0.1708	0.0854	1.96	0.29	0.0138	6018	590	3528
625	0.1582	0.0791	1.7	0.22	0.0076	18360	1138	6804
550	0.1392	0.0696	1.39	0.15	0.0034	86193	2829	16915
500	0.1265	0.0633	1.2	0.11	0.0017	301543	5915	35364

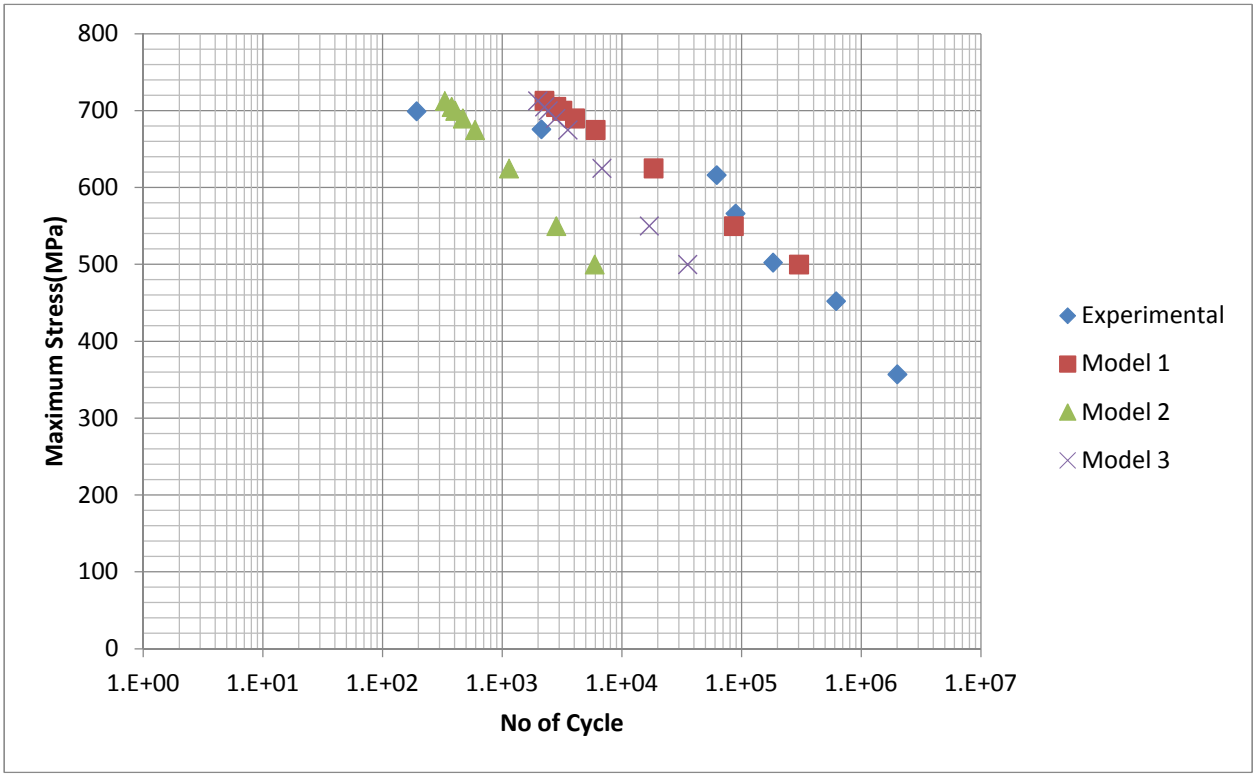

Figure 4. 12: Comparison of three model data with experimental data for R=0.5

In Figure [4.12] model 1 is matching properly with the experimental data. Experimental points are slightly in and out form the model curve with similar slope. Also from the model adequacy analysis, model 1 is showing least error fit with the experimental data.

Among all of this graph best fit are selected for each ratio. Model adequacy checking was done for the best fit. Eqn (4.5) was used for model adequacy [22].

$$e = | \sum (y_i - y_j) | \qquad \text{Eqn (4.5)}$$

Here, y_i stands for experimental value and $y_j$for model value.

Table 4. 7: Best parameters for each ratio, R=0.1, 0.3, 0.5

R	C	$\frac{\gamma_f'}{y_y}$	e
0.1	0.2	1	20080
0.3	0.3	1	90300
0.5	0.53	1	110280

From this table we see that as the value of ratio increases, C also increases with a constant value of $\frac{\gamma_f'}{y_y}$.

4.5 Power Law Model

The Power law model for high cycle fatigue data is shown in Eqn (4.6)

$$S = AN_f^n \qquad \text{Eqn (4.6)}$$

In logarithmic form

$$log\, S = n log\, N_f + \beta \qquad \text{Eqn (4.7)}$$

where,

$$A = 10^{\beta} \qquad \text{Eqn (4.8)}$$

$$n = \alpha \qquad \text{Eqn (4.9)}$$

From the experimental data, regression analysis is desirable.

Table 4. 8: Regression analysis of each R.

R		Coef-ficients	Standard Error	t Stat	P-value	Lower 95%	Upper 95%	Lower 95.0%	Upper 95.0%
0.1	β	3.523	0.142	24.838	0.002	2.913	4.133	2.913	4.133
	α	-0.172	0.026	-6.596	0.022	-0.284	-0.060	-0.284	-0.060
0.3	β	3.439	0.136	25.234	0.002	2.853	4.025	2.853	4.025
	α	-0.155	0.025	-6.121	0.026	-0.264	-0.046	-0.264	-0.046
0.5	β	3.452	0.092	37.396	0.001	3.055	3.849	3.055	3.849
	α	-0.141	0.016	-8.554	0.013	-0.212	-0.070	-0.212	-0.070
0.7	β	3.118	0.031	101.160	0.000	2.986	3.251	2.986	3.251
	α	-0.072	0.006	-12.872	0.006	-0.096	-0.048	-0.096	-0.048

After the regression analysis, with the value of α and β for each ratio predicted S-N curve was drawn. They are shown in following Figures [4.13-4.16].

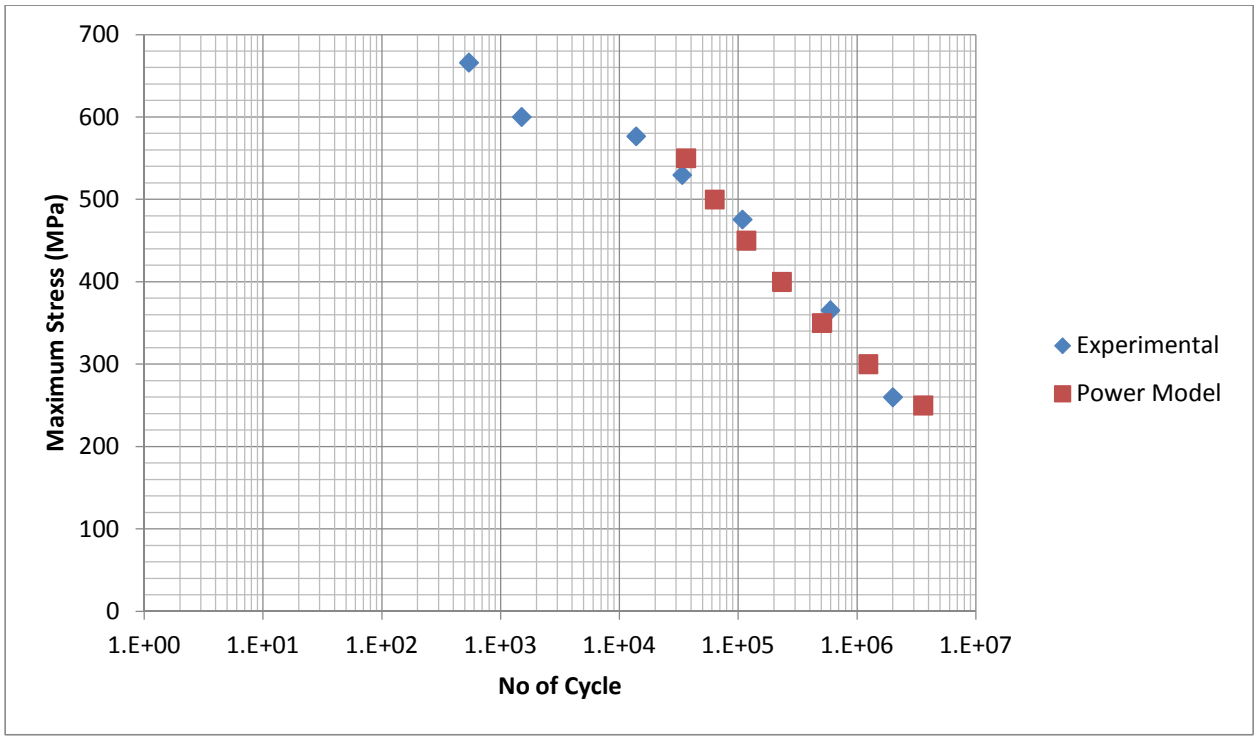

Figure 4. 13**: Power Law model with experimental value for R=0.1**

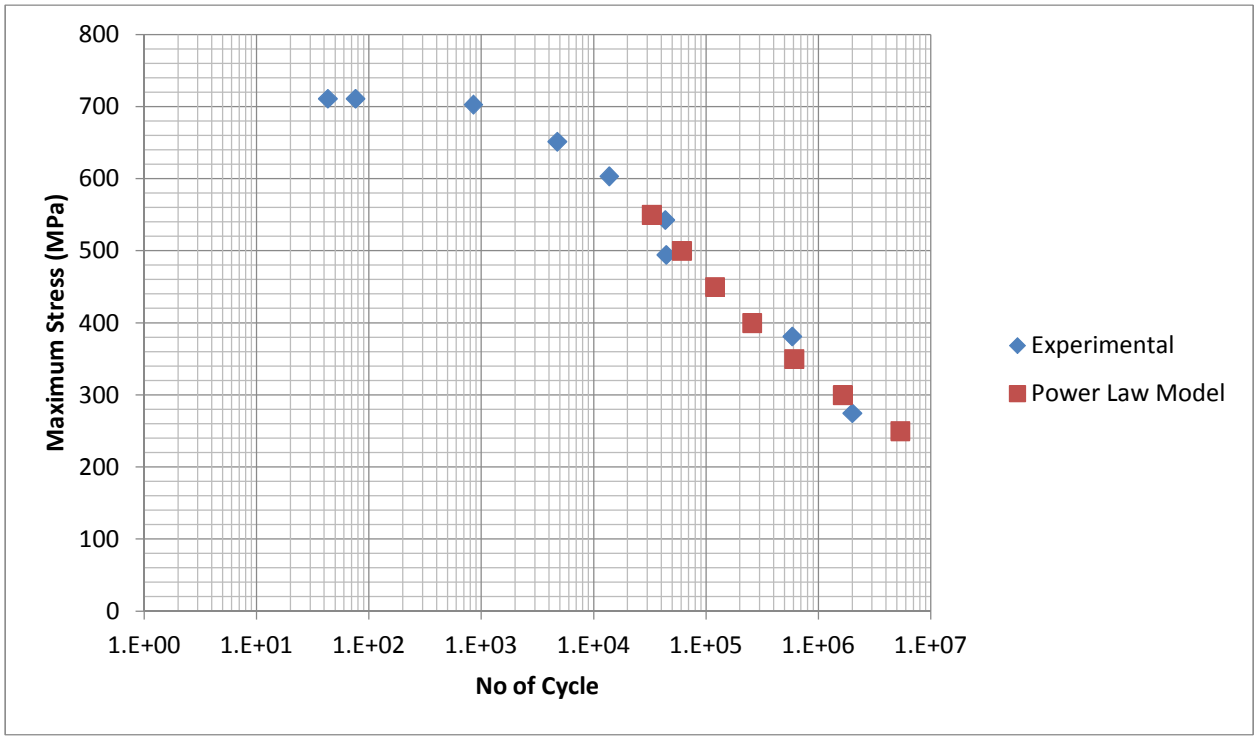

Figure 4. 14: Power Law model with experimental value for R=0.3

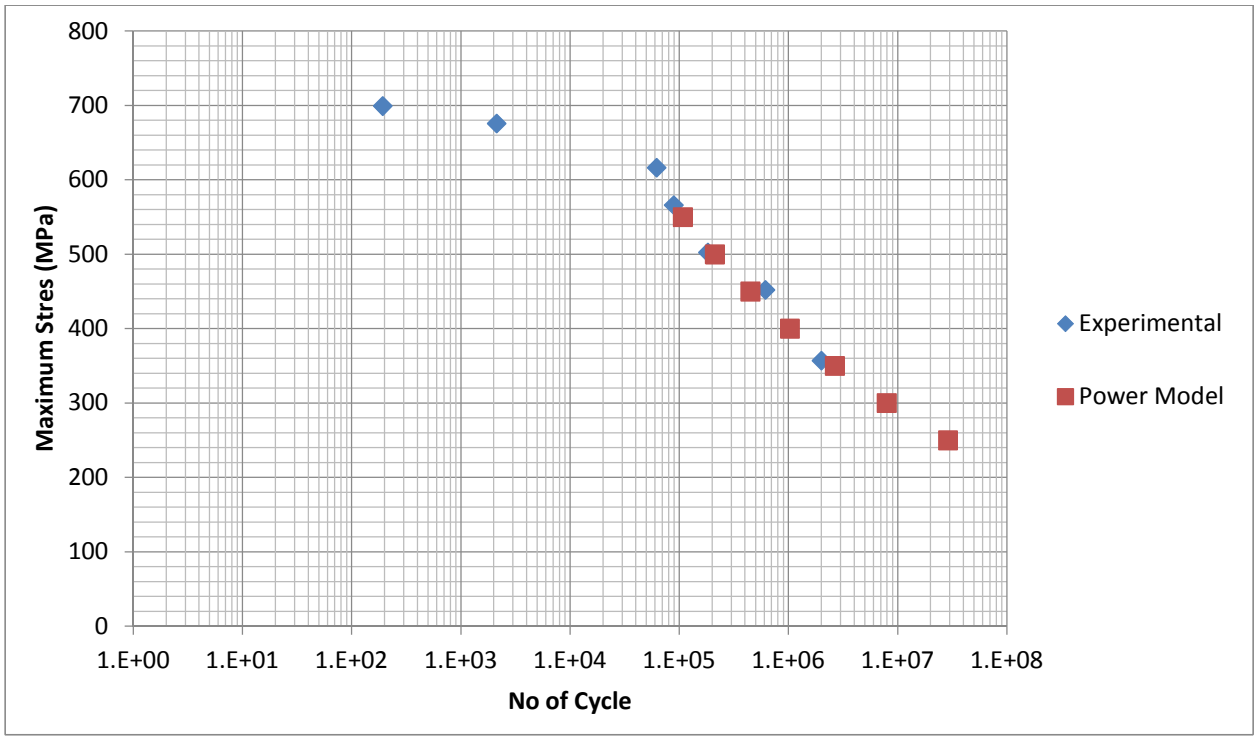

Figure 4. 15: Power Law model with experimental value for R=0.5

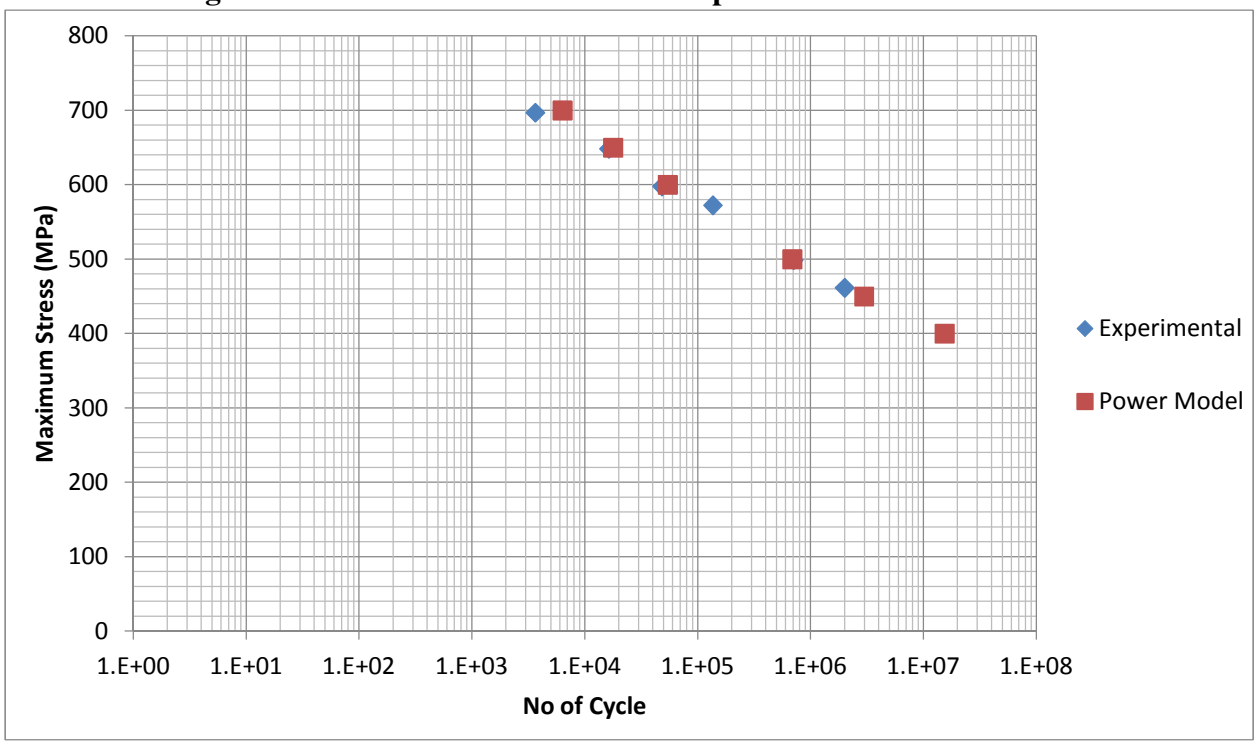

Figure 4. 16: Power Law model with experimental value for R=0.7

Figures [4.17-4.19] show the high cycle (Power Law model) and low cycle (Slaughter-Fleck's model) with experimental data for each value of R.

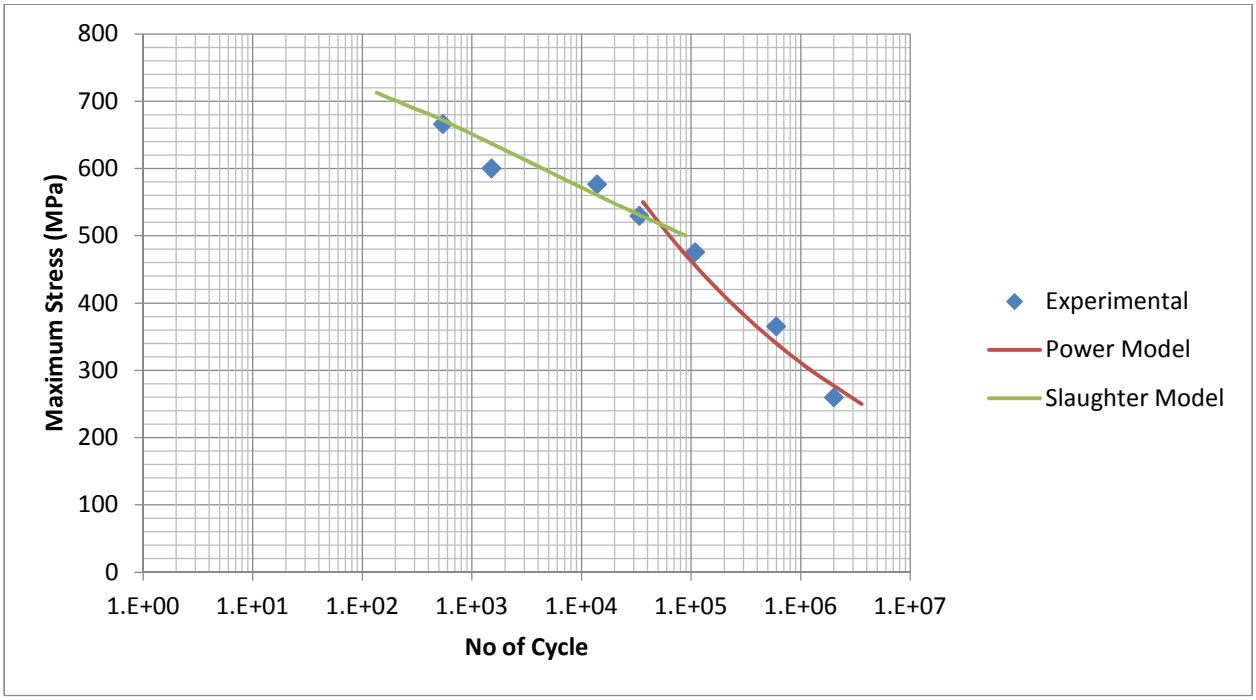

Figure 4. 17: Both high and cycle model with experimental data of R=0.1

In Figure [4.17], Salughter-Fleck's model for R=0.1, is showing a good agreement with experimental data as discussed for Figure [4.10].

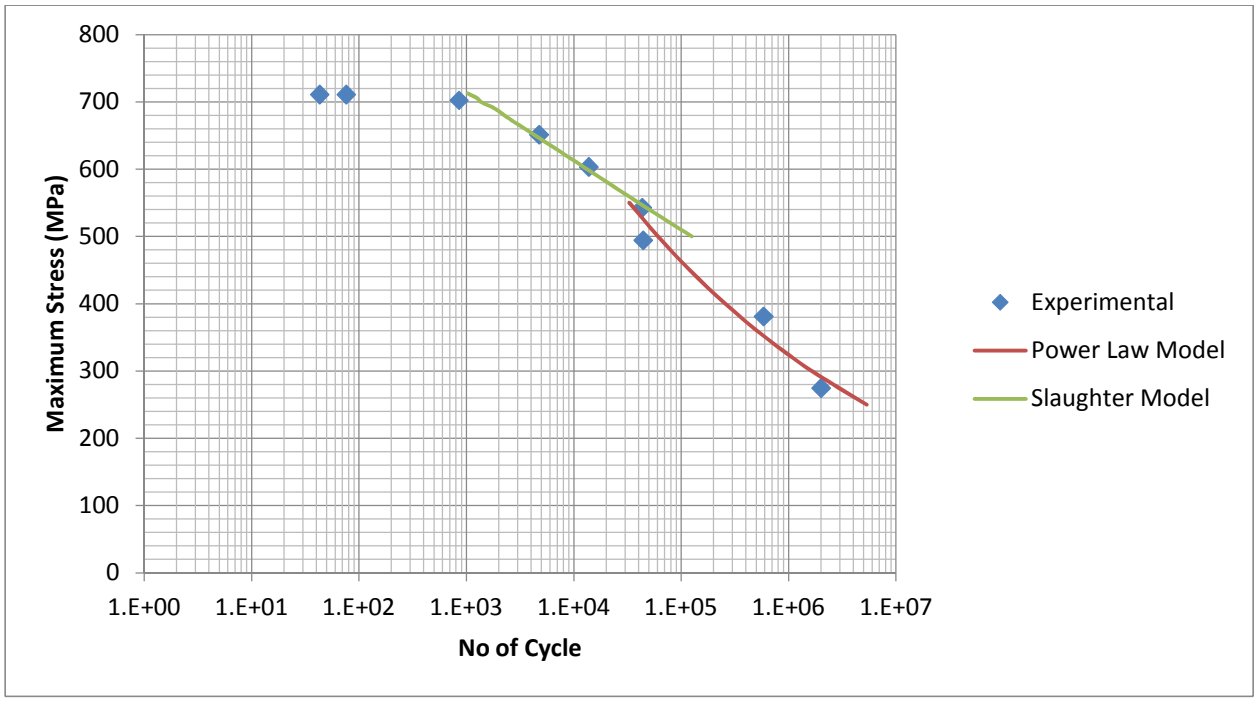

Figure 4. 18: Both high and cycle model with experimental data of R=0.3

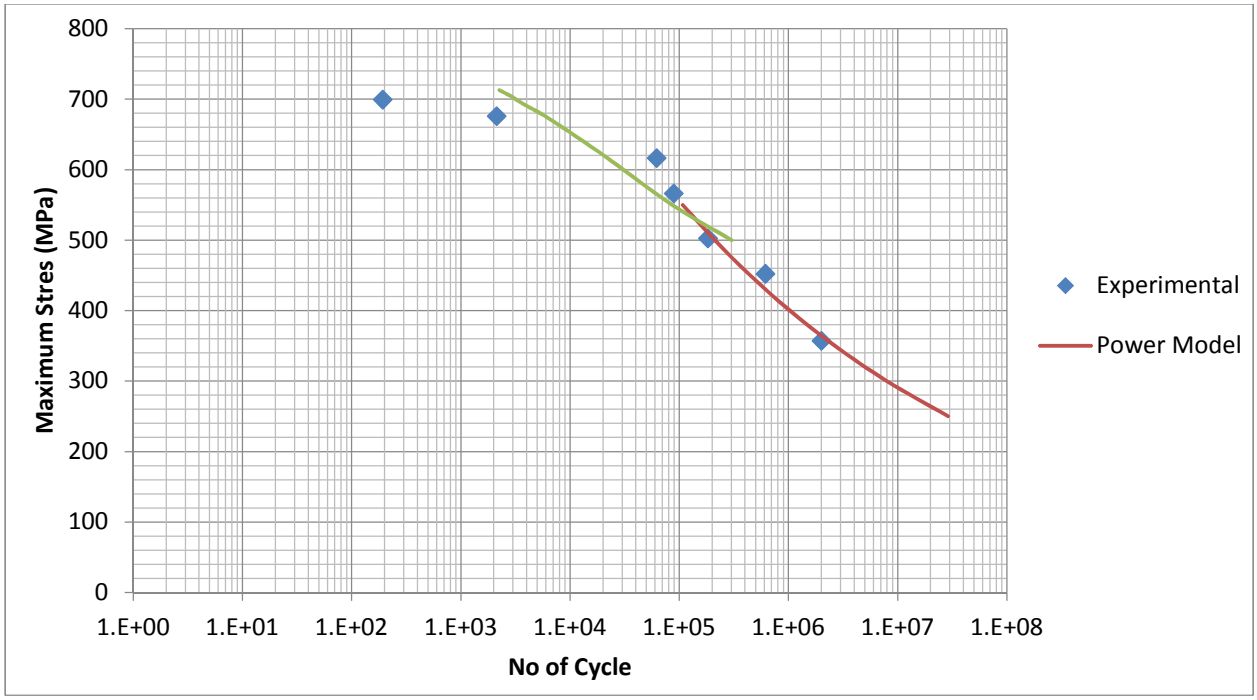

Figure 4. 19: Both high and cycle model with experimental data of R=0.5

Figures [4.17-4.19] show the both low and high cycle model with experimental data. Both models are showing good agreement with the experimental data of their cycle region. Low cycle region that represents compressive failure and high cycle region that represents tensile failure are coinciding at around 500 MPa.

4.6 Image Processing

Pictures were taken of the compression and tension surface of all samples after fracture. Image processing was used to assess the amount of damage on both the tensile and compression faces. Pixels of each picture were converted into gray value. Thresholding was then applied to each picture. Figure [4.20-4.21] show the compression and tension surfaces of R=0.1. In each figure, images at the left show the actual specimen surface and the images at right side show the processed image. They are presented from the highest maximum stresses at the top of the figure to lowest maximum stress at the bottom.

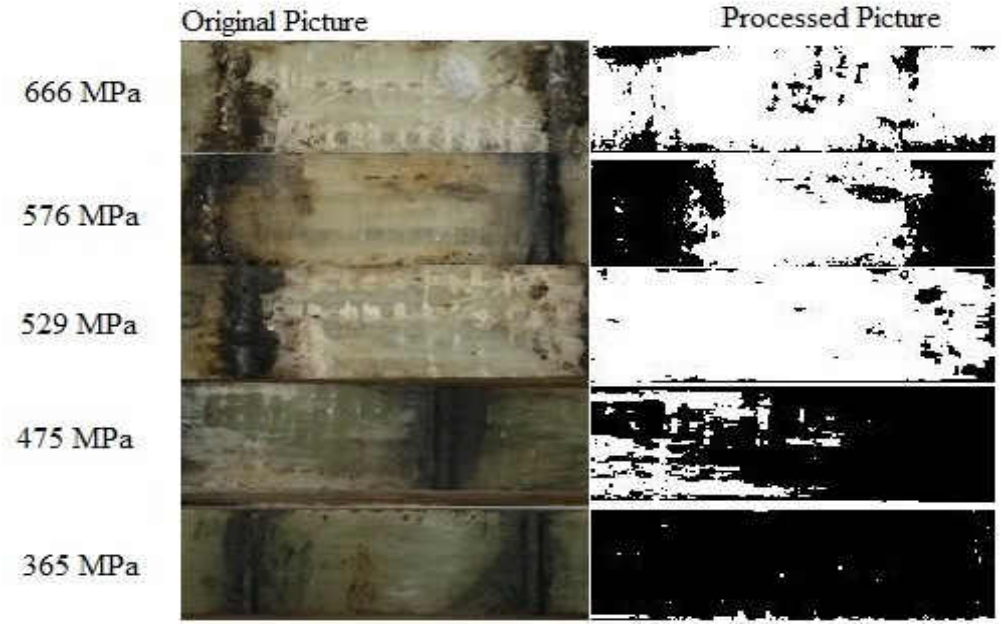

Figure 4. 20: Compression surface for R=0.1

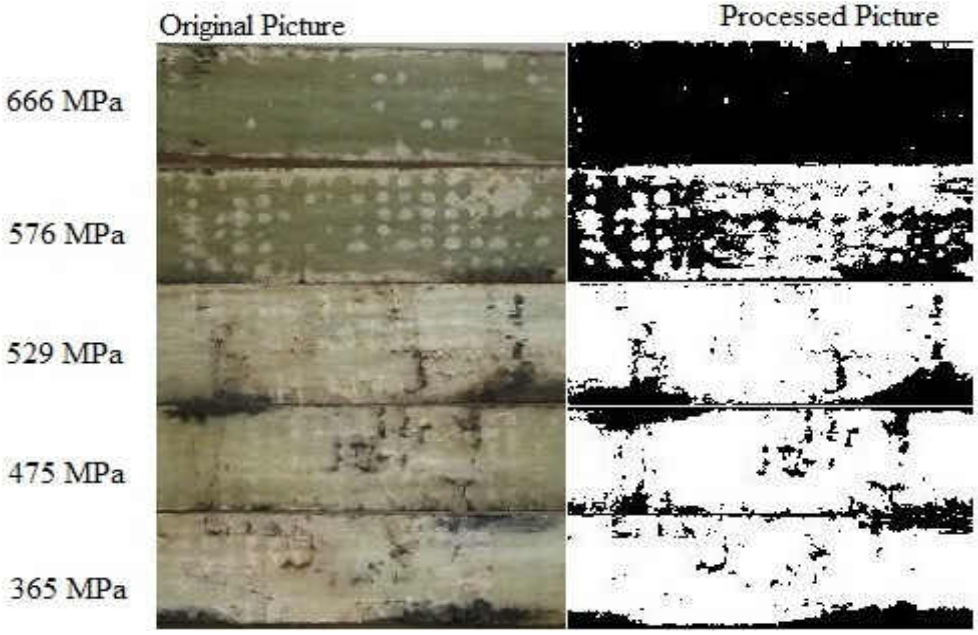

Figure 4. 21: Tension surface for R=0.1

Fractured surface failure in Figure [4.20] is larger in Samples from 666 MPa to 572 MPa than in samples from 475 MPa to 365 MPa. Tension surface in Figure [3.21], the samples from 529 MPa to 365 MPa are containing larger fracture than in the samples from 666 MPa to 576 MPa. The middle sample of 529 MPa are containing a significant amount of fracture both in tension and compression surface.

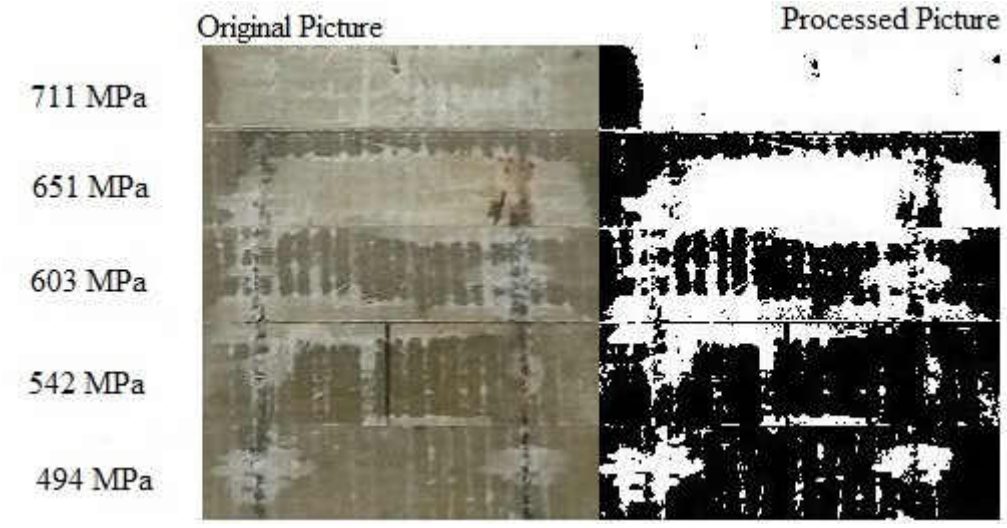

Figure 4. 22: Compression surface for R=0.3

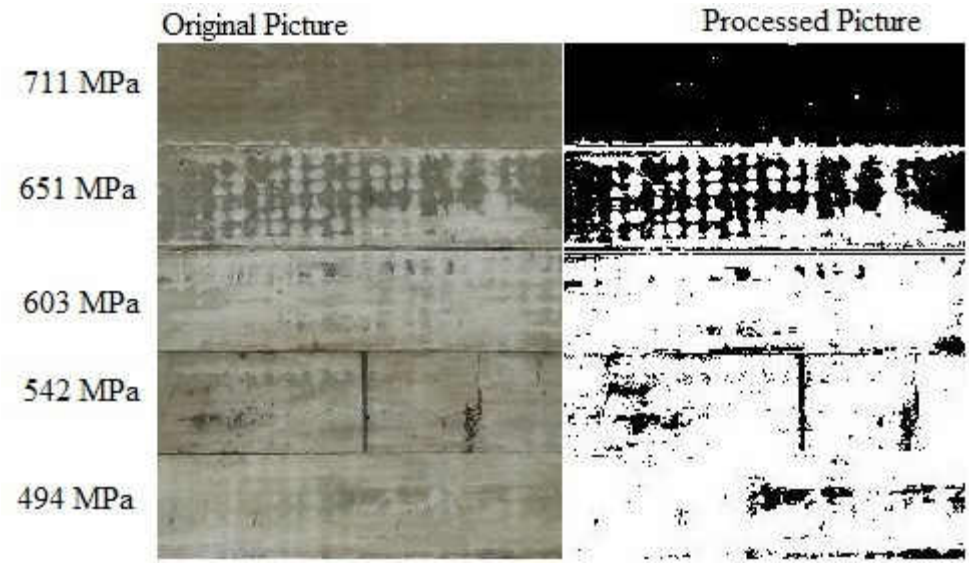

Figure 4. 23: Tension surface for R=0.3

Fractured surface failure in Figure [4.22] is larger in Samples from 711 MPa to 651 MPa than in samples from 603 MPa to 494 MPa. Tension surface in Figure [4.23], the samples from 603 MPa to 494 MPa are containing larger fracture than in the samples from 711 MPa to 651 MPa.

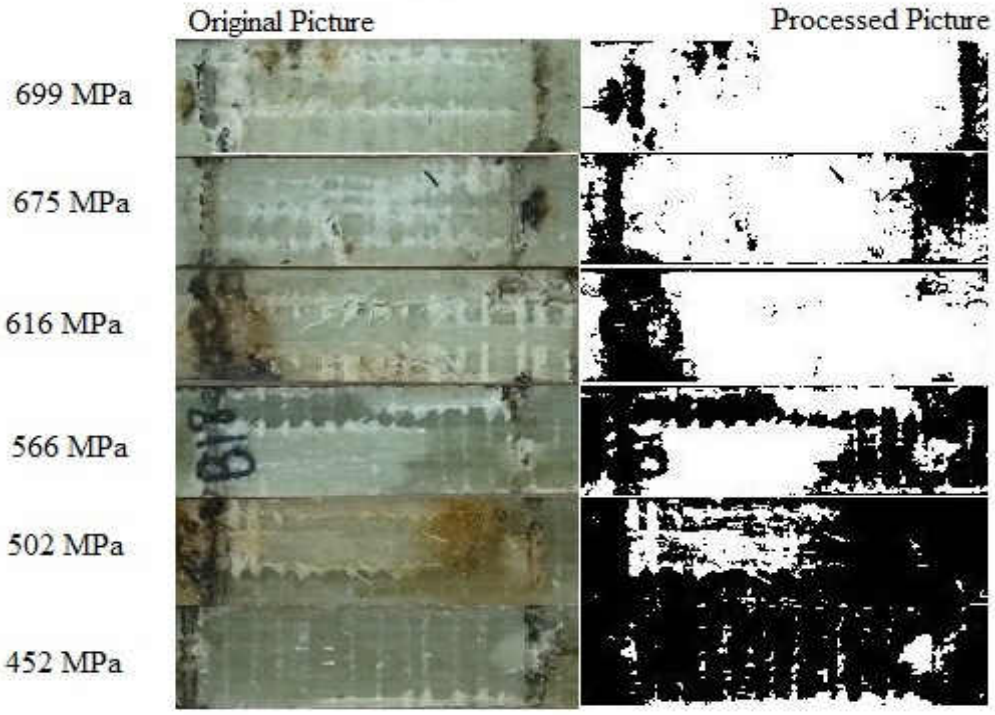

Figure 4. 24: Compression surface for R=0.5

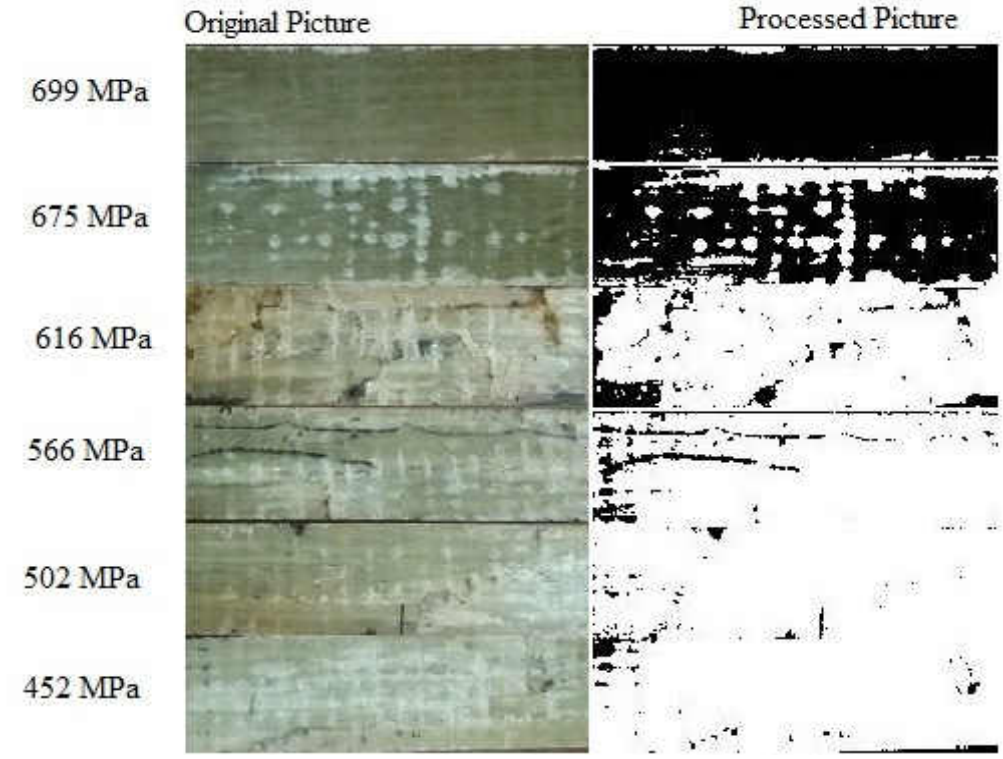

Figure 4. 25: Tension surface for R=0.5

Fractured surface failure in Figure [4.24] is larger in Samples from 699 MPa to 616 MPa than in samples from 566 MPa to 452 MPa. Tension surface in Figure [4.25], the samples from 616 MPa to 452 MPa are containing larger fracture than in the samples from 699 MPa to 675 MPa. The sample of 616 MPa are containing a significant amount of fracture both in tension and compression surface.

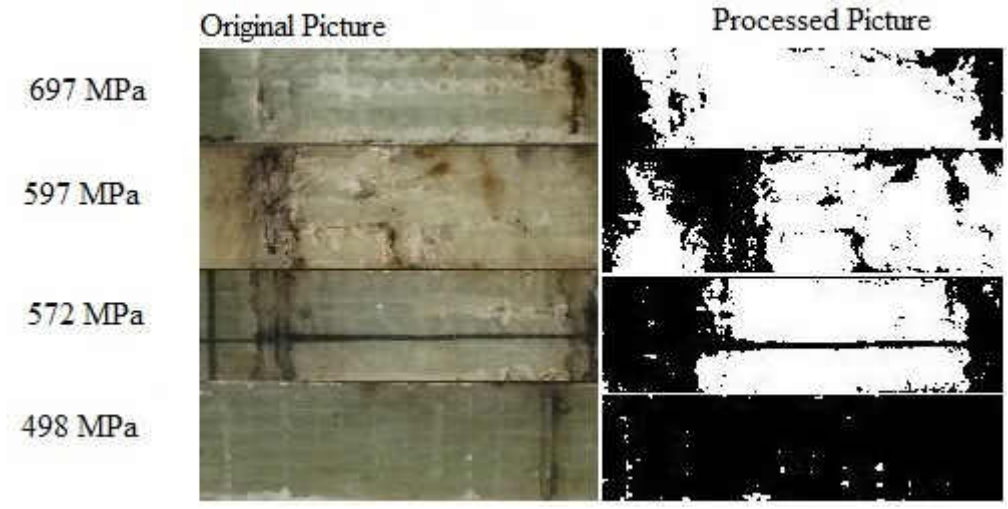

Figure 4. 26: Compression surface for R=0.7

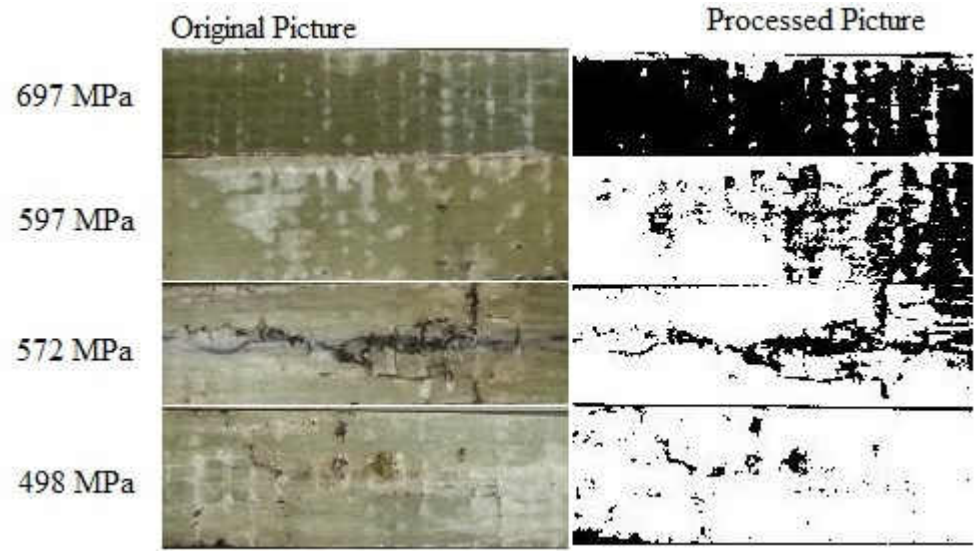

Figure 4. 27: Tension surface for R=0.7

Fractured surface failure in Figure [4.26] is larger in Samples from 697 MPa to 572 MPa than in sample of 498 MPa. Tension surface in Figure [4.27], the samples from 597 MPa to 498 MPa are containing larger farcture than in the samples of 697 MPa. The samples of 597 MPa and 572 MPa are containing a significant amount of fracture both in tension and compression surface.

Figures [4.20-4.27] show a relation between applied stress and fractured area in each sample. When the applied stress is decreased fracture observed on the compression surface also decreases. However, the transition is not smooth and not in same stress region for ration to ratio. Image processing was done in Matlab. Black area represents non-fractured material and white regions represent fractured/delaminated area in the Figures [4.20-4.27]. From Matlab, the no of pixels in each area (Black, White) can be determined. Figures [4.28-4.36] show the fractured area fraction vs Maximum stress. The portion of the samples that were taken for image processing is the area between the load span.

Fractured area Fraction = no of pixels for black area/total no of pixels for the original picture Eqn (4.10).

Figures [4.28-4.29] stand for compression and tension surface, respectively, of R=0.1.

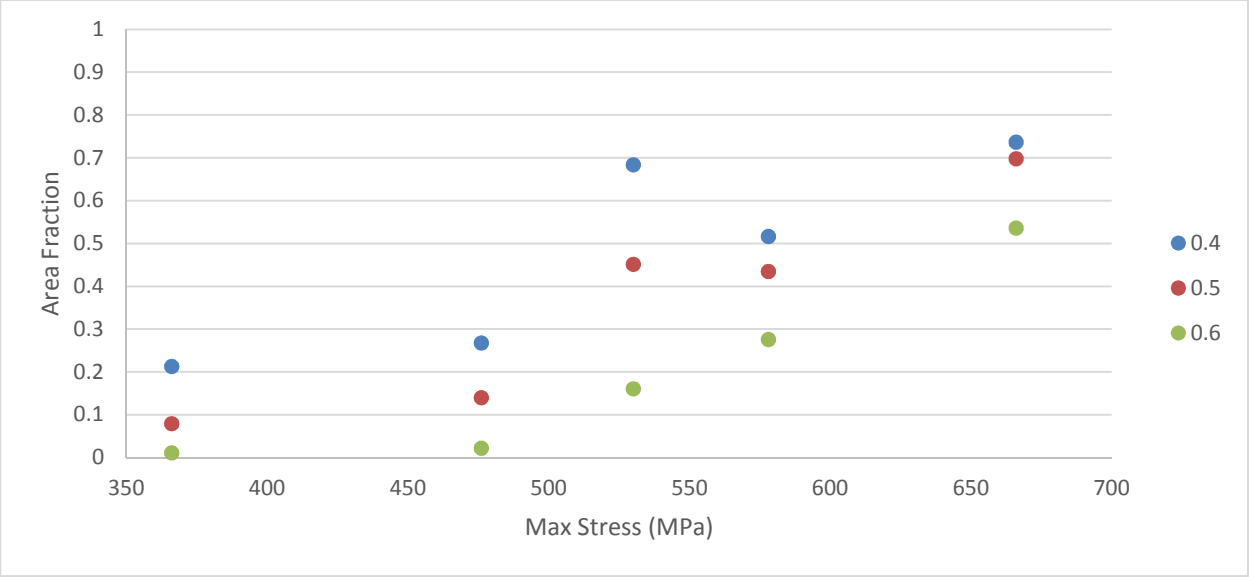

Figure 4. 28: Fractured area fraction of compression surface for R=0.1 vs imaging threshold value

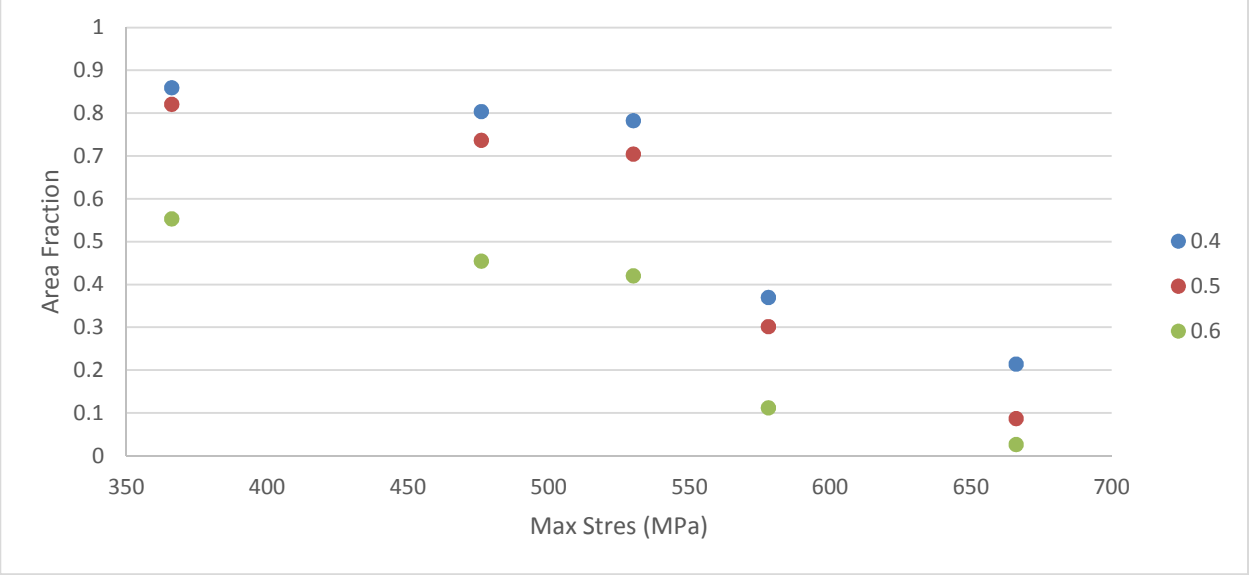

Figure 4. 29**: Fractured area fraction of tension surface for R=0.1 vs imaging threshold value**

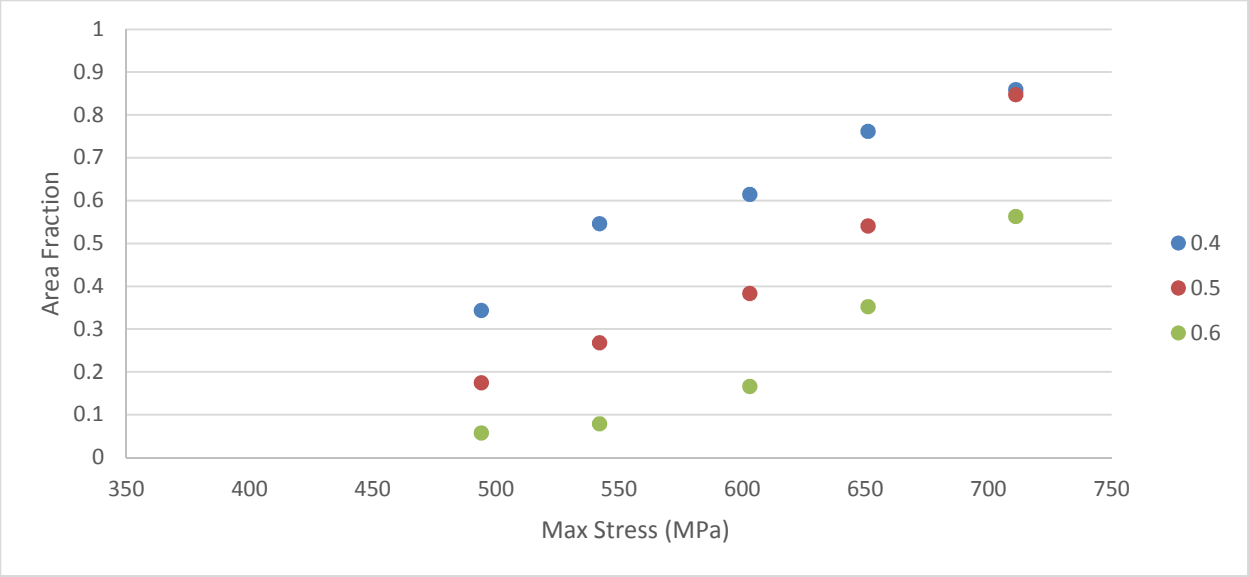

Figure 4. 30: Fractured area fraction of compression surface for R=0.3 vs imaging threshold value

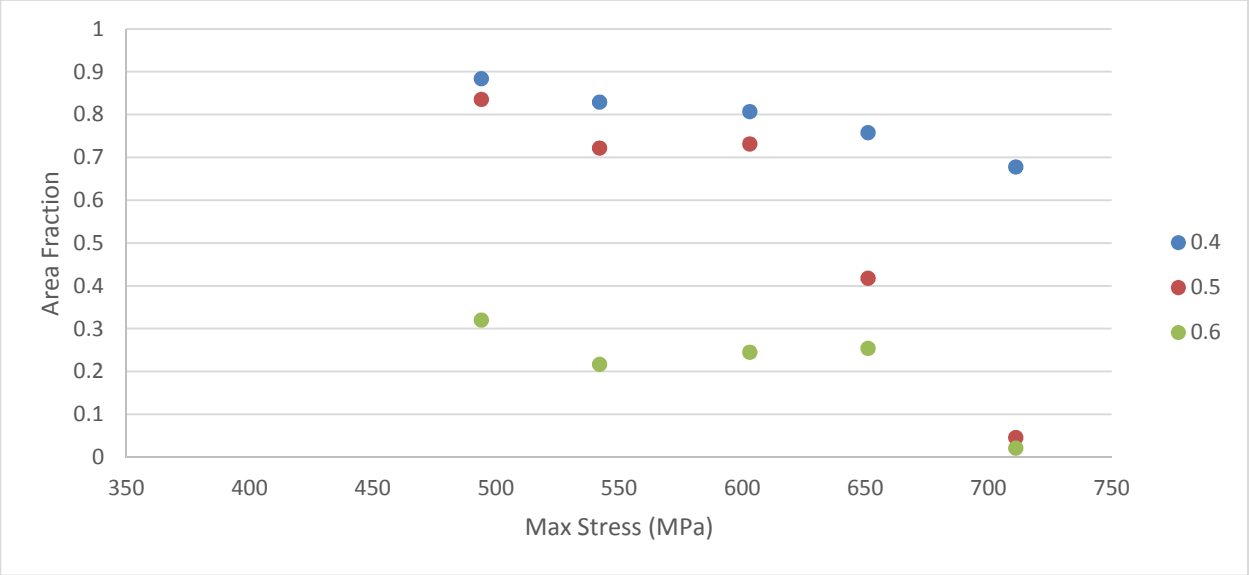

Figure 4. 31: Fractured area fraction of tension surface for R=0.3 vs imaging threshold value

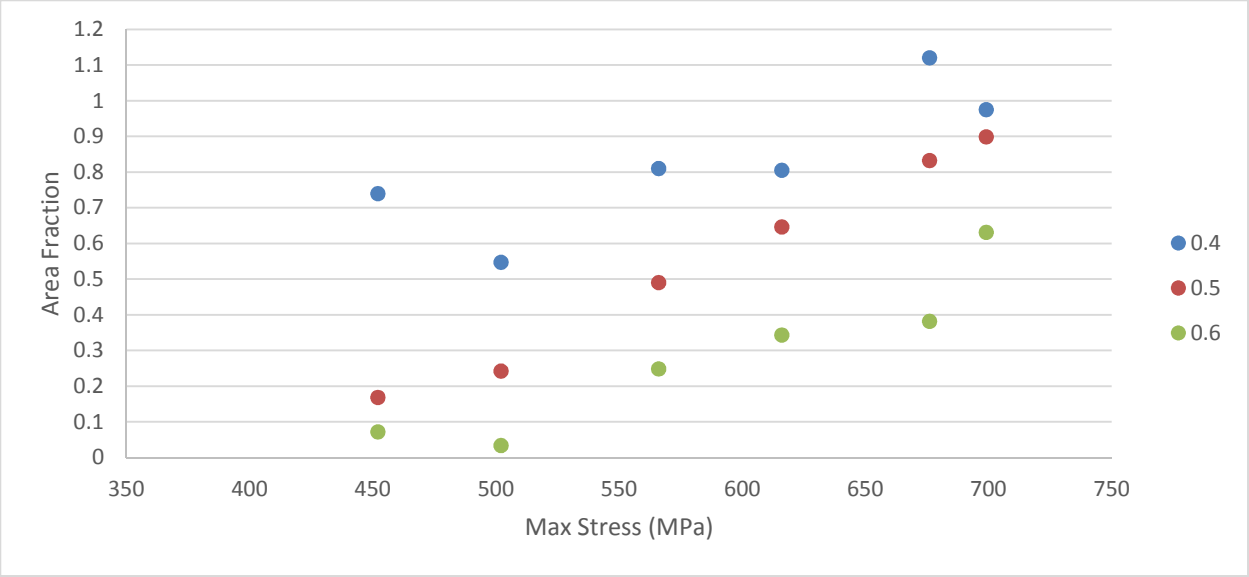

Figure 4. 32: Fractured area fraction of compression surface for R=0.5 vs imaging threshold value

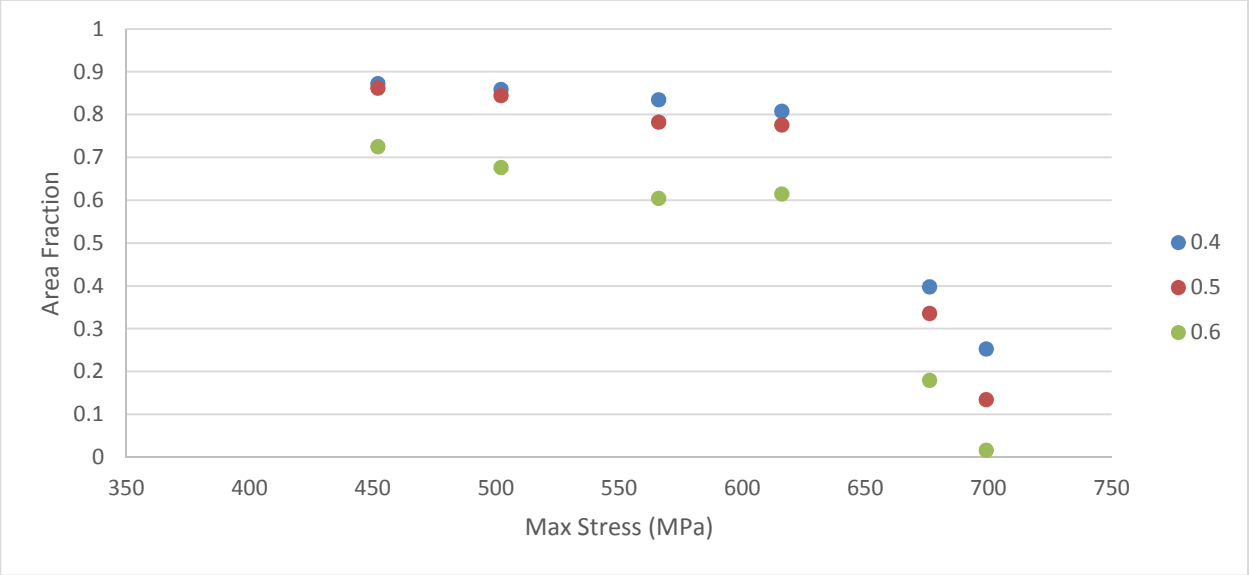

Figure 4. 33: Fractured area fraction of tension surface for R=0.5 vs imaging threshold value

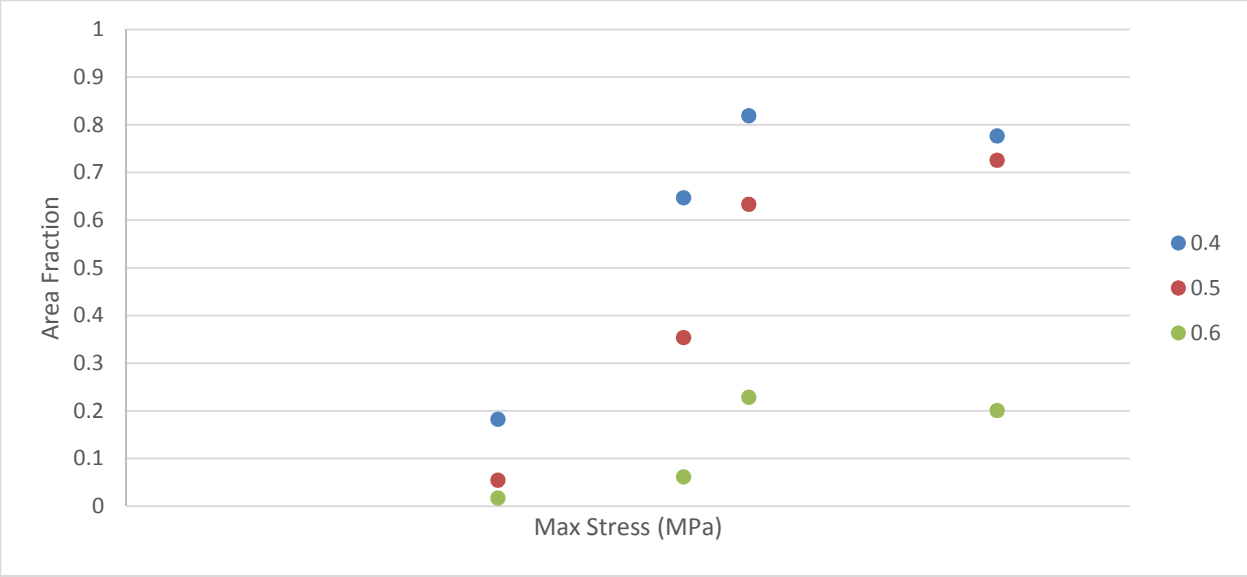

Figure 4. 34: Fractured area fraction of compression surface for R=0.7 vs imaging threshold value

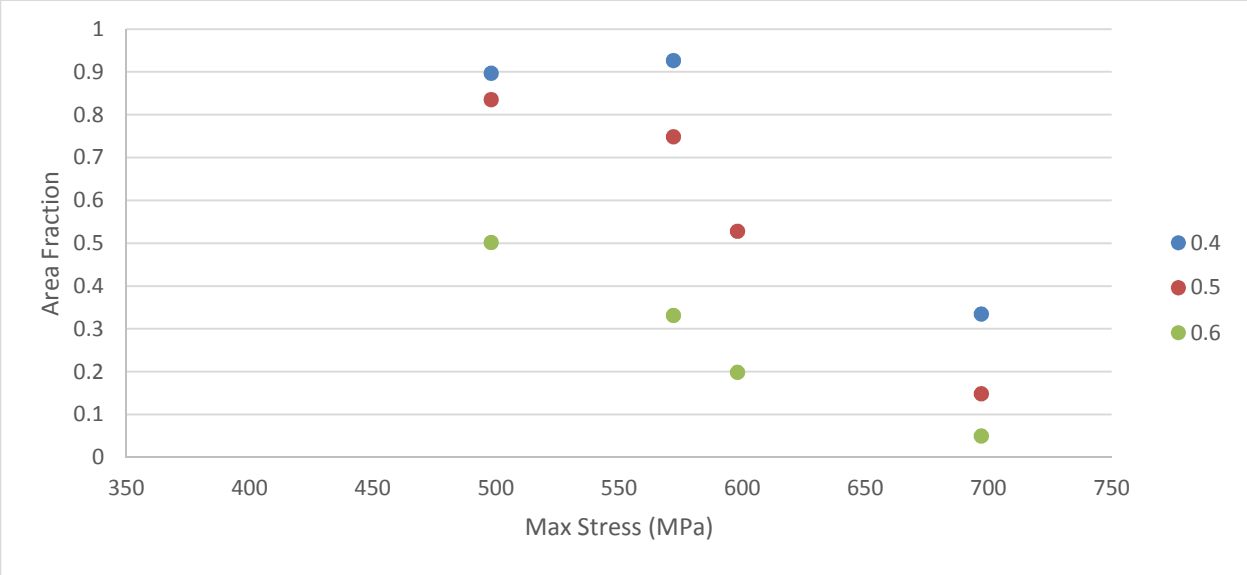

Figure 4. 35: Fractured area fraction of tension surface for R=0.7 vs imaging threshold value

The observation that has already discussed for Figures [4.21-4.26] is supporting by these Figures [4.27-4.35]. The quantifying value for fractured in surface area has determined approximately by threshold value of 0.5. The processed pictures of each samples was shown is Figures [4.21-4.27] are processed by this value of threshold.

Additional graph has drawn to total damage in surface that is summation of fracture quantity of tension and compression surface. Figures [4.36-4.39] are representing the overall fracture for each ration for 0.5 threshold parameter as it is the best threshold value.

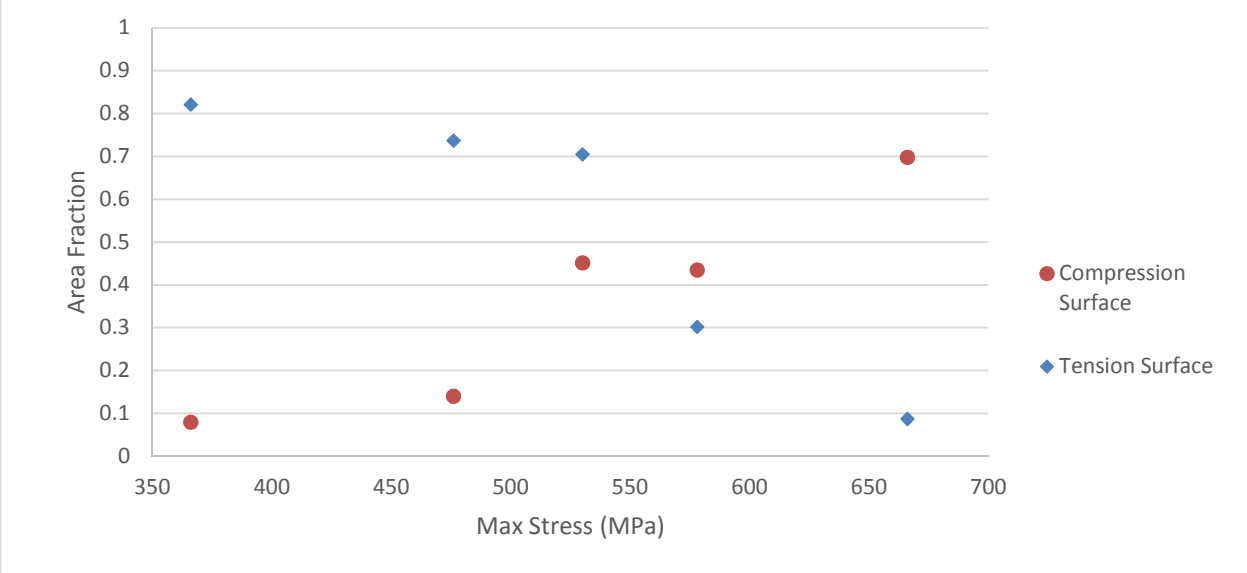

Figure 4. 366: Fractured area fraction of both surface for R=0.1 vs imaging threshold value

From Figure [4.36-4.39], it can be concluded that each sample for any stress were contain around 43%-450% surface failure combined in tension and compression surface.

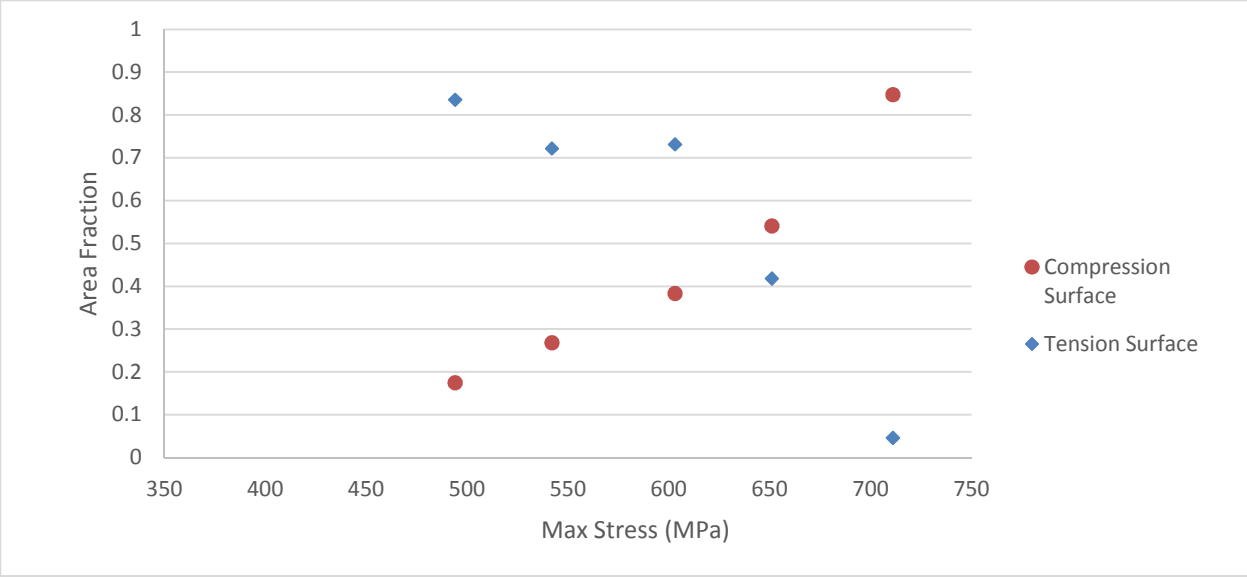

Figure 4. 377: Fractured area fraction of both surface for R=0.3 vs imaging threshold value

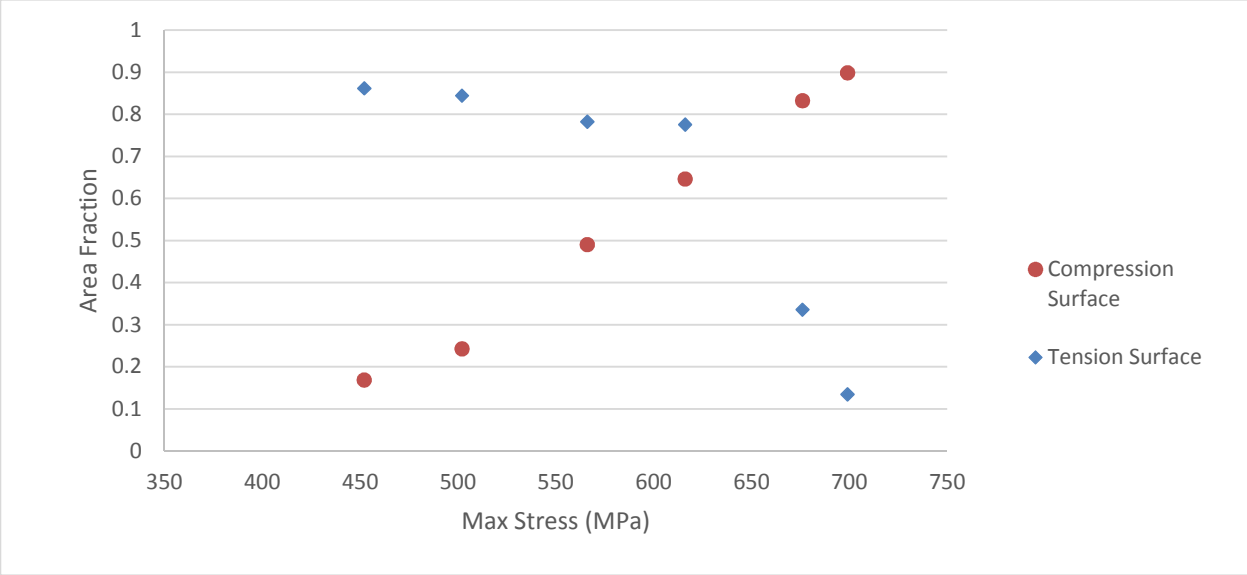

Figure 4. 388: Fractured area fraction of both surface for R=0.5 vs imaging threshold value

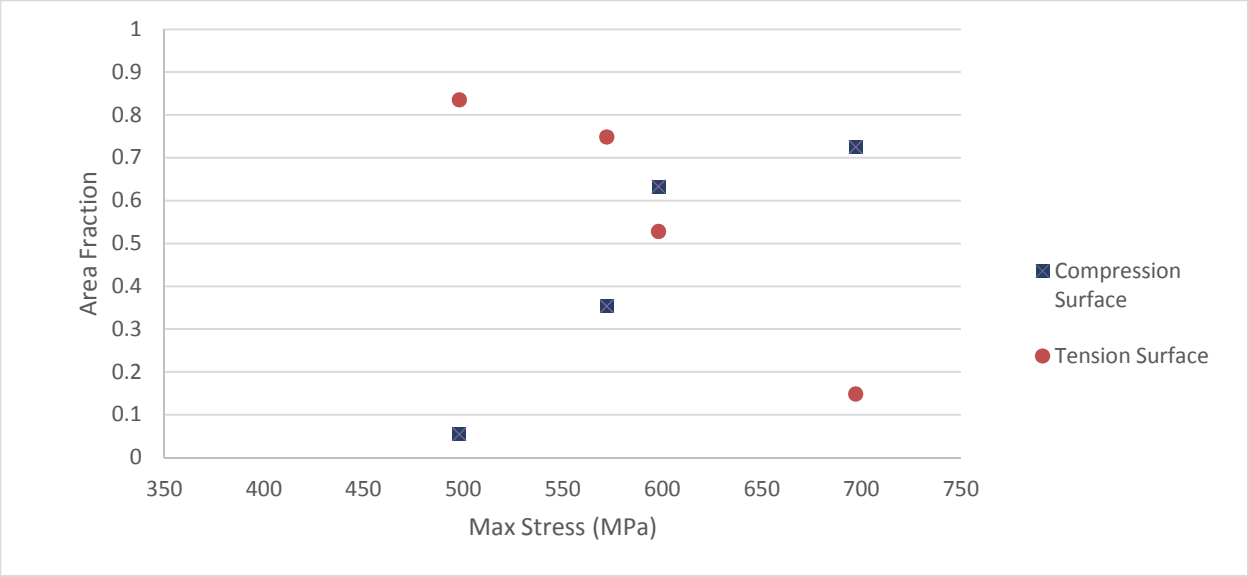

Figure 4. 399: Fractured area fraction of both surface for R=0.7 vs imaging threshold value

4.7 Replication

After all the analysis completed, we have tested four samples for replication at R=0.3 below table is showing that data

Table 4. 9: Fatigue data for replicates

Ratio,R	Sample Name	Length,L (mm)	Thickness,b (mm)	Width, d (mm)	Maximum Stress (MPa)	Cycle
0.3	F12	203.2	8.70	25.76	626.5	8131
	F13	203.2	8.71	25.51	381.9	412381
	F7	203.2	8.62	24.98	546.7	57467
	F2	203.2	8.51	25.65	492.0	151424

S-N curve for R = 0.3 with the replication values are in below.

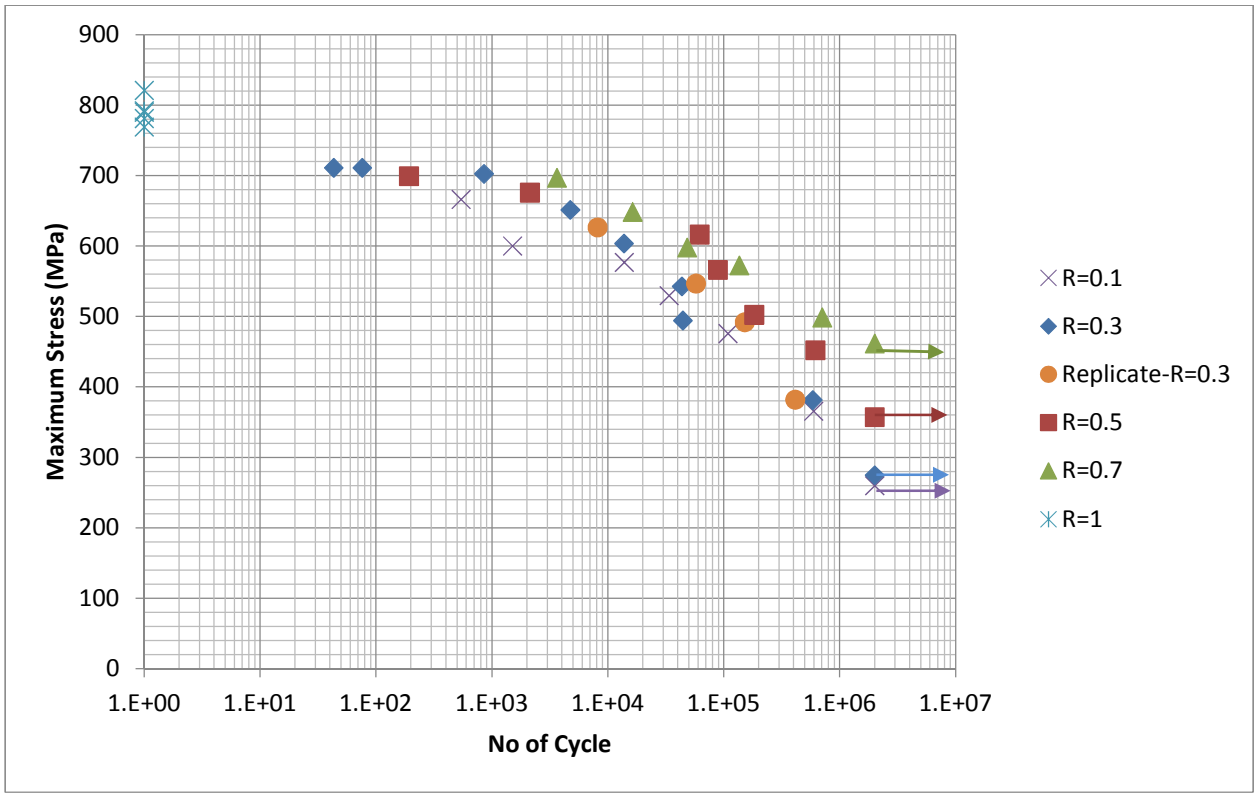

Figure 4.40: S-N curve with replicate

Replication values are showing good similarities with the previous data of R=0.3. On an average to make this data set more plausible at each point at least three data should be replicated. For this replication it would be best option to design an experiment with 5-7 stress level and 3 replicates. Before started this study design of experiment was not applied here due to lack of knowledge. After findings it is not convenient in time respect to replicate all the data. But obviously for future study it will be wise decision to conduct a design of experiment with proper replication point.

CHAPTER FIVE: CONCLUSION

The purpose of this study was to study the fatigue behavior of glass fiber composites in four point bending. The materials used here were supplied by LM Wind Power. Sample beams were fabricated by VARTM (Vacuum Assisted Resin Transfer Molding). To make the samples compatible with the capacity of fatigue test machine, ten layers of fiber are used. The goal was to conduct 4 point bending fatigue tests for positive load ratios. Load ratios used were 0.1, 0.3, 0.5, and 0.7. All the fatigue tests were run at the same loading frequency (5 Hz) and using a sinusoidal curve.

From this study designers can give insights about the fatigue of glass fiber composites that can be applied their products after a certain period of time. The conclusions in this study are 1) fracture under tensile stress is more likely than buckling under compression stress in bending dominated high life cycle product design, 2) two empirical models from the literature, one each for low cycle and high cycle fatigue region, can be used to predict fatigue lifetime for corresponding maximum stress and stress ratio without full experiment investigations and 3) from stiffness degradation analysis, predictions about the service lifetimes of products can be made.

This study shows that at high stress, close to ultimate flexural strength of a material, product's failure is prone to buckling at the compression surface by local bending stress. Designers or fatigue inspectors can get an idea about the loading condition after investigating failures of parts. May be that loading condition was not included in the design and also maybe the loading

condition was not frequent. With the result of this study and inspection results, a designer can start further investigations to find out the potential loading behavior that should not be in the actual application. This work showed the transition from compression surface failure to tension surface failure occurred in between 67% to 78% of ultimate flexural strength of the composite materials.

From the stiffness degradation analysis, engineers can predict when a material is going to fail for a particular design condition if there is no other uncertainty. Flexural stiffness was calculated throughout the fatigue test. Normalized Flexural Modulus vs Normalized Cycle to Failure plot shows that the change in stiffness is very slow in the first 80%-90% of the fatigue life of each sample. After that, the stiffness decreases very fast throughout the rest of life. If we know the design stress and corresponding lifetime then we can say for this particular condition the material is safe for at least 80% of its predicted lifetime.

When the data was stored in computer, the sampling frequency must be defined. For this study it was 1 in 100/cycle. My recommendation is for the high cycle-low stress region it is enough but for low cycle-high stress region each cycle should be stored. The reason is that in the low cycle-high stress region the stiffness is degraded in the 50 cycle-100 cycles. If all data is not stored then it will be difficult to construct the full degradation curve.

Finally, the associated empirical models will be valuable to predict fatigue lifetimes. High cycle fatigue region and low cycle fatigue region is divided here by the approximate maximum applied stress 500 MPa. There is a different characteristic equation for each region of the fatigue curve equations. Low cycle fatigue can be predicted by Slaughter Fleck's model and high cycle fatigue by the power law model.

Further study can be done for reverse load ratios, different numbers of plies, different initiator percentages and different support and load span. Also, there are some potential recommendations for the future findings to improve the results and process. It will be good to take an image of each surface from each sample before and after the fatigue test. This will give better comparison data in the image analysis packages. Applying a design of experiments methodology will be great for any further study. It will be minimize the replication quantity and increase confidence in the data and findings.

Appendix A

Sample Name	Hardness	Sample Name	Hardness	Sample Name	Hardness
A1	85.2	B1	87.0	D1	90.2
A2	85	B2	90.3	D2	88.7
A3	87.7	B3	86.3	D3	91.8
A4	91.8	B4	92.2	D4	86.5
A5	91.1	B5	85.5	D5	89.6
A6	91	B6	90.2	D6	88.4
A7	88	B7	89.6	D7	84.8
A8	89	B8	86.4	D8	90.9
A9	86.2	B9	85.2	D9	85.4
A10	88.7	B10	89.3	D10	85.9
A11	88.6	B11	87.4	D11	88.3
A12	91.0	B12	88.5	D12	91.8
A13	89.5	B13	84.8	D13	86.9
A14	88.7	B14	90.2	D14	90.8
A15	91.6	B15	89.7	D15	87.5
A16	91.6	B16	90.2	D16	85.8
A17	91.7	B17	89.7	D17	90.3
A18	87.9	B18	85.7	D18	86.9

References

[1] R. F. Gibson, Principles of Composite Material Mechanics, New York: CRC Press, 2012.

[2] M. C. K. Mayers, Mechanical Behavior of Materials, Cambridge: Cambridge University Press, 2013.

[3] A. a. Y. N. Makeev, "Fatigue Life Assesment of Composite Structure," in *Proceedings of the 26th ICAF Symposium*, Montreal, 2011.

[4] K. a. S. S. Momenkhani, "A New Method for Predicting the Fatigue Life of Fiber Reinforced Plastic Laminates," *Journal of Composite Materials,* vol. 38(10), pp. 1971-1982, 2005.

[5] G. e. a. Labeas, "Adaptive Progressive Damage Modeling for Large-Scale Composite Structure," *International Journal of Damage Mechanics,* vol. 21, pp. 441-462, 2012.

[6] M. a. H. S. Kawai, "Effects of Non-Negative Mean Stress on the Off-Axis Fatigue Behavior of Unidirectional Carbon/Epoxy Composites at Room Temperature," *Journal of Composite Materials,* vol. 38(10), pp. 833-854, 2004.

[7] A. H. H. a. P. M. Varvani-Farahani, "A Fatigue Damage Parameter for Life Assesment of Off-Axis Unidirectional GRP Composite," *Journals of Composite Materials,* vol. 40(18), pp. 1659-1670, 2006.

[8] ASTM D2344, "Standard Test Method for Apparent Interlaminar Shear Strength of Parallel Fiber Composites by Short-Beam Method," *ASTM,* 2000.

[9] R. Hibbler, Mechanics of Materials, Pearson, 2011.

[10] E. a. T. E. Hanus, "Influence of Four-Point Bending Fatigue on The Residual Stress State of a Pressure Rolled, Particulate-Reinforced Metal Matrix Composite," *Materials Science and Engineering A,* vol. 194, pp. 147-156, 1995.

[11] S. e. a. Subramanian, "A Cumulative Damage Model to Predict the Fatigue Life of Composite Laminates Including the Effect of Fiber-Matrix Interphase," *Internatial Journal of Fatigue,* vol. 17(5), pp. 434-351, 1995.

[12] F. a. W. Y. Wu, "A Fatigue Damage Model of Composite Materials," *International Journal of Fatigue,* vol. 58, pp. 134-138, 2010.

[13] H. a. S. M. Mao, "Fatigue Damage Modeling of Composite Materials," *Composite Structure,* vol. 58, pp. 405-410, 2002.

[14] W. e. a. Shi, "A Damage Mechanics Model for fatigue Life Prediction of Fiber Reinforced Polymer Composite Lamina," *Acta Mechanica Solida Sinica,* vol. 24(5), pp. 399-410, 2011.

[15] M. a. R. H. Owen, "Accumulation of Damage of Glass-Reinforced Plastic Under Tensile and Fatigue Loading," *Journal of Physics D: Applied Physics,* vol. 5, pp. 1937-1953, 1972.

[16] J. a. P. C. Epssrachchi, "An Empirical Model for Fatigue Behavior Prediction of Glass Fiber-Reinforced Plastic Composites for Various Stress Ratios and Test frequencies," *composites: Part A,* vol. 34, pp. 313-326, 2003.

[17] K. a. S. S. Momenkhani, "Devlopment and Application of a Model Using Center of Gravity Hysterisis Loops to Predict Fatigue Damage Accumulation in Fiber-Reinforced Plastic Laminates," *Journal of Composite materials,* vol. 39(6), pp. 557-575, 2005.

[18] M. Reimbayev, "Fatigue Behavior of Continuous Fiber-Reinforced Composite Beam," University of North Dakota, Grand Forks, 2012.

[19] N. Dowling, "Mean Stress Effects in Stress-Life and Strain-Life Fatigue," *SAE Technical Paper,* vol. 01, pp. 2216-2227, 2004.

[20] B. a. N. F. Budianski, "Compressive Failure of Fiber Composites.," *Journal of the Mechanics and Physics of Solids,* vol. 41(1), pp. 183-211, 1993.

[21] W. a. N. F. Slaughter, "Compressive Fatigue of Fiber Composites," *Journal of Mechanics and Physics of Solids,* vol. 41(8), pp. 1265-1284, 1993.

[22] L. Devore, Modern Mathematical Statistics with Application, Springer, 2011.

[23] R. e. a. Sadeghian, "Manufacturing Carbon Nano-Fibers Toughtened Polyester/Glass Fiber Composite Using Vacuum Assisted Resin Transfer Molding for Enhancing The Mode I Delamination Resistance," *ELSEVIER,* pp. 1787-1795, 2005.

[24] ASTM D3171, "Standard Test Method for Constituent Content of Composite Materials," *ASTM,* 2009.

[25] ASTM D6272-10, "Standard Test Method for Fluxural Properties of Uninforced and Reinforced Plastics and Electrical Insulation Materials by Four-Point Bending," 2010.

[26] W. a. H. K. Hawang, "Cumulative Damage models of multi stress Fatigue Life Prediction," *Journal of Composite Materials,* vol. 20(2), pp. 125-153, 1986.

[27] J. e. a. Howson, "Fatigue Performance of Marine Laminates Reinforced With Kevlar Aramid Fibers," in *Composites International Conference and Exhibition*, Paris.

[28] J. e. a. Yang, "A Stiffness Degradation Model for Graphite Epoxy Laminates," *J. Comp. Technol. Res.,* vol. 11(4), pp. 129-134, 1990.

[29] A. e. a. Makeev, "Manufacturing Issues and Measuement Techniques for Assesment of the Effects on Structural Performance of Composite Parts," in *Proceedings of the AHS 66th Annual Forum*, Phoenix, 2010.

[30] H. a. D. H. Hahn, "Fatigue Behavior of Composite Laminates," Washington University, St. Louis, 1981.

[31] J. a. a. Halpin, "Characteristics of Composites for The Purpose of Reliability Prediction, Analysis of Test Methods for High Modulus Fibers and Composites," *ASTM STP,* p. 521, 1973.

[32] Y. e. al, "The Effect of Load Sequence on Statistical Fatigue of Composites," *AIAA J,* vol. 18(12), pp. 1525-1531, 1980.

[33] y. e. al, "Load Sequence Effects on Graphite/Epoxy Laminates in Long-Term Behavior of Composites," *ASTM STP,* vol. 813, pp. 246-262, 1983.

[34] e. a. Yang., "Load Sequence Effects on the Fatigue of Unnotched Composite Materials in Fatigue of Fibrous Composite Materials," *ASTM STP,* vol. 723, pp. 213-231, 1981.

[35] B. RD, "An up-and-down procedure for acute toxicity testing," 1985. [Online]. Available: http://www.ncbi.nlm.nih.gov/pubmed/3987991.